Performance Analysis of RIS-Assisted Cell-Free Massive MIMO Systems with Transceiver Hardware Impairments

Yao Zhang, *Member, IEEE*, Wenchao Xia, *Member, IEEE*, Haitao Zhao, *Senior Member, IEEE*, Gan Zheng, *Fellow, IEEE*, Sangarapillai Lambotharan, *Senior Member, IEEE*, and Longxiang Yang

***Abstract*—Integrating reconfigurable intelligent surface (RIS) into cell-free massive multiple-input multiple-output (MIMO) is a promising approach to enhance the coverage quality, spectral efficiency (SE), and energy efficiency. In this paper, an RIS-assisted cell-free massive MIMO downlink system suffering from the transceiver hardware impairments (T-HWIs) is investigated. To improve the accuracy of the direct estimation (DE) scheme, a modified ON/OFF estimation (MOE) with moderate pilot overhead is proposed. Relying on the knowledge of imperfect channel state information, we derive closed-form expressions of the lower-bound achievable SE with T-HWIs under both DE and MOE schemes. The closed-form results facilitate the investigation of how RIS improves the downlink SE under various system settings and allow us to explore the trade-off strategies between using more hardware-impaired APs and low-cost RISs in terms of the downlink SE and power consumption. Numerical results validate the theoretical analysis and show that the proposed MOE scheme outperforms the DE scheme in terms of the downlink SE. Moreover, the benefits of introducing RIS into hardware-impaired cell-free massive MIMO systems are also illustrated.**

***Index Terms*—Cell-free massive multiple-input multiple-output (MIMO), reconfigurable intelligent surface (RIS), transceiver hardware impairments (T-HWIs), channel estimation, performance analysis.**

I. Introduction

As a potential candidate technology for future sixth-generation (6G) communications, cell-free massive multiple-input multiple-output (MIMO) is attracting growing interest for its ability to tackle the inter-cell interference and poor quality-of-service (QoS) of cell-edge user equipments (UEs) issues in cellular massive MIMO systems [1]–[5]. However, the performance of cell-free massive MIMO systems is still highly prone to deteriorate in unfavorable propagation environments, such as sparse scattering scenarios and long-distance/obstructive propagation losses.

A disruptive technology, breaking through the limitation, has emerged under the label of reconfigurable intelligent surface (RIS) or intelligent reflecting surface (IRS) [6]–[8]. An RIS typically consists of a large number of hardware-efficient passive scattering elements, which can individually manipulate the phase shifts of incident signals without requiring a dedicated power amplifier as needed in amplify-and-forward relaying systems, thus facilitating low-power, massive-connectivity, energy-efficient, high-spectral efficiency (SE), and low-latency communications [9]–[11]. It has been proved that configuring RIS in cellular massive MIMO systems under the imperfect channel state information (CSI) can ameliorate the poor channel propagation and significantly improve the QoS of all UEs [12]–[14]. As a consequence, the integration of the RIS and the state-of-the-art cell-free massive MIMO system has attracted much interest in recent years.

A. Related Works

Relying on the knowledge of imperfect CSI, recent studies have explored the RIS-assisted cell-free massive MIMO system under different scenarios and demonstrated its advantages over the conventional cell-free massive MIMO system without RIS in terms of the SE and EE performance. For instance, in [15], Nahhas et al. estimated the aggregated channel using the direct estimation (DE) scheme and analyzed the achievable SE of an RIS-assisted cell-free massive MIMO system with single-antenna access points (APs) and sufficient orthogonal pilots. Simulation results demonstrated that using RIS is energy-efficient and improves the SE of the UE with poor direct channel propagation. Considering the impact of the pilot contamination, Chien et al. [16] analyzed both uplink and downlink SE performance under spatially correlated RIS channels, suggesting that the correlation between RIS elements may not affect the SE unless the RIS phase shifts are optimized. Nadeem et al. [17] studied the UE fairness in an RIS-assisted cell-free massive MIMO uplink system and proposed a joint max-min SE optimization algorithm that takes into account the receiver combining weights, power control coefficients,

The work of Wenchao Xia, Haitao Zhao, and Longxiang Yang was supported in part by the National Key Research and Development Program of China under Grant 2020YFB1806608, in part by the Jiangsu Natural Science Foundation for Distinguished Young Scholars under Grant BK20220054, in part by the Natural Science Foundation on Frontier Leading Technology Basic Research Project of Jiangsu under Grant BK20212001, in part by the National Natural Science Foundation of China under Grants 62071246 and 62201285, and in part by the China Postdoctoral Science Foundation under Grant 2022M722669. The work of Gan Zheng and Sangarapillai Lambotharan was supported by the Royal Society under the International Exchanges Cost Share NSFC Award under Grant IEC\NSFC\211209. The work of Yao Zhang was supported by the Zhejiang Provincial Natural Science Foundation of China under Grant LQ23F010010. Corresponding Authors: Haitao Zhao, Wenchao Xia.

Y. Zhang is with the College of Physics and Electronic Information Engineering, Zhejiang Normal University, Jinhua 321004, China. E-mail: zhangyao94@126.com.

G. Zheng is with the School of Engineering, University of Warwick, CV4 7AL Coventry, United Kingdom. E-mail: gan.zheng@warwick.ac.uk.

S. Lambotharan is with the Wolfson School of Mechanical, Electrical, and Manufacturing Engineering, Loughborough University, Loughborough LE11 3TU, United Kingdom. E-mail: s.lambotharan@lboro.ac.uk.

W. Xia, H. Zhao, and L. Yang are with the Department of Wireless Communication Key Lab of Jiangsu Province, Nanjing University of Posts and Telecommunications, Nanjing 210003, China. E-mail: xiawenchao@njupt.edu.cn, zhaoht@njupt.edu.cn, yanglx@njupt.edu.cn.

and RIS phase shifts. Simulations revealed that the proposed algorithm outperforms the benchmark algorithms that optimize one or two types of these parameters. In [18], Nguyen et al. designed a hybrid Relay-RIS architecture in which a small number of passive elements are substituted with active processing units and pointed out that the proposed hybrid Relay-RIS architecture achieves a significant improvement in the SE performance over the pure passive RIS architecture at the cost of increased power consumption. Note that [15]–[18] all used the DE scheme, which minimizes the pilot overhead but degrades the accuracy of the channel estimation. Bashar et al. [19] designed an ON/OFF estimation (OE) scheme that estimated the indirect RIS-assisted channel sequentially and proposed an efficient max-min SE optimization algorithm with respect to the RIS phase shifts under zero-forcing receivers. Compared with the DE scheme, the OE scheme achieves a higher estimation accuracy but requires more coherent samples for uplink training, thus leading to a lower transmission efficiency. Unlike [15]–[19], the authors in [20]–[23] paid attention to the EE optimization under perfect CSI scenarios. In [20], Zhang et al. proposed a hybrid beamforming strategy to maximize the downlink EE by decomposing the beamforming into the AP-based digital beamforming and the RIS-based analog beamforming. Taking into account the backhaul limitations, Le et al. [21] presented an efficient alternating algorithm to maximize the downlink EE. Lyu [22] et al. considered the hybrid Relay-RIS architecture and proposed a EE maximization algorithm in terms of the transmit beamforming coefficients and RIS phase shifts. Moreover, focused on the uplink, Liu et al. [23] formulated a EE fairness problem and determined its solution by virtue of the Lagrangian transform and fractional programming. To summarize, all results showed that the RIS can substantially improve the SE and EE performance of cell-free massive MIMO systems.

In aforementioned RIS-aided cell-free massive MIMO systems, the APs and UEs with ideal/high-quality hardware are unrealistic and may incur in high implementation cost and energy consumption. An RIS-assisted cell-free massive MIMO architecture is attractive when the APs and UEs are configured with non-ideal/low-quality hardware [24]–[26]. Non-ideal transceivers are energy-efficient but introduce hardware impairments (such as the amplifier nonlinearities, phase noise, in-phase/quadrature-phase imbalance, quantization noise, etc.) that degrade the benefits accrued from cell-free massive MIMO systems. The error vector magnitude (EVM) model can well capture the impact of transceiver hardware impairments (T-HWIs), which suggests that the transmitted or received signal is distorted by an additive Gaussian noise that is uncorrelated with the data signal [26]. The impact of T-HWIs on the SE and EE performance of cell-free massive MIMO systems without RIS has been extensively investigated in [27]–[31]. As expected, the results showed that the T-HWIs are determinant factors that decrease the SE in the high signal-to-noise ratio (SNR) regime. Although increasing the AP density or the number of antennas per AP can counterbalance the SE degradation that arises from T-HWIs, this method induces additional implementation cost and power consumption, and is in general, not a desirable approach. A more efficient performance compensation technique is imperatively needed. We note that since the RIS can provide substantial SE gain at a relatively low cost, it is appealing to use the RIS to alleviate the impact of T-HWIs and enhance the SE performance of all UEs. The existing related works that studied the SE performance of RIS-aided wireless communication systems with T-HWIs, to the best of our knowledge, all focused on the perfect CSI assumption or small-scale communication scenarios [32]–[35]. There is no work in technical literature that explores the feasibility and effectiveness of using RIS in hardware-impaired cell-free massive MIMO systems under the imperfect CSI and quantitatively investigates its impact. Such observation motivates this work.

B. Contributions

In this work, our aim is to reveal the impact of RIS on a hardware-impaired cell-free massive MIMO downlink system. A modified OE (MOE) scheme is proposed to balance the channel estimation accuracy and the pilot overhead. Relying on the knowledge of imperfect CSI, closed-form expressions of the lower-bound achievable SE under DE and MOE schemes in the presence of T-HWIs are derived, which enable us to quantitatively analyze the impact of key parameters and draw some system-design guidelines. The technical derivation under the non-Gaussian aggregated channel, imperfect CSI, different estimation schemes, any finite numbers of APs/UEs/RISs/elements per RIS, and T-HWIs requires considerable mathematical analyses and makes this work non-trivial and novel. In summary, the main contributions of this paper are outlined as follows.

1) We investigate the impact of RIS on a hardware-impaired cell-free massive MIMO downlink system and establish a framework to quantify the channel estimation and SE performance under imperfect CSI and T-HWIs using the EVM model. This is the first work to conduct such an investigation.
2) A MOE scheme is proposed to balance the channel estimation accuracy and the pilot overhead. We derive closed-form expressions of the lower-bound achievable SE for arbitrary numbers of APs/UEs/RISs/elements per RIS. The closed-form expressions are proven to be tight and facilitate the analysis of the impact of key parameters on both downlink SE and power consumption.
3) We demonstrate by simulations that the MOE scheme reaps a lower normalized mean square error of the channel estimation (NMSE-CE) and a higher achievable SE than the DE scheme. Besides, the UE HWIs degrade the downlink SE significantly but can be mitigated by deploying a few RISs. Regardless of the degree of T-HWIs, the RIS-assisted cell-free massive MIMO system has much higher SE than the system without RIS, especially when the RISs are located near the UEs. Moreover, the APs can reduce their transmit power to the milliwatt level with negligible SE loss when using RIS.
4) The trade-off strategies between using more hardware-impaired APs and low-cost RISs in terms of the downlink SE and power consumption are explored. We find

TABLE I
MAJOR NOTATIONS

Notation	Description
M	Number of APs
K	Number of UEs
J	Number of RISs
N	Number of antennas of each AP
L	Number of elements of each RIS
$\boldsymbol{g}_{mk}$	Aggregated channel from AP_m to UE_k
$\boldsymbol{g}^c_{mkjl}$	Cascaded channel between AP_m and UE_k via RIS_{jl}
$\boldsymbol{g}^d_{mk}$	Direct channel from AP_m to UE_k
$\boldsymbol{g}^d_{mjl}$	Direct channel from RIS_{jl} to AP_m
g^d_{kjl}	Direct channel from RIS_{jl} to UE_k
β_{mk}	Large-scale fading coefficient of $\boldsymbol{g}_{mk}$
β^c_{mkj}	Large-scale fading coefficient of $\boldsymbol{g}^c_{mkjl}$
β^d_{mk}	Large-scale fading coefficient of $\boldsymbol{g}^d_{mk}$
β^d_{mj}	Large-scale fading coefficient of $\boldsymbol{g}^d_{mjl}$
β^d_{kj}	Large-scale fading coefficient of g_{kjl}
f_{jl}	Frequency response of RIS_{jl}
α_{jl}	Amplitude reflection coefficient RIS_{jl}
θ_{jl}	phase shift of RIS_{jl}
τ_p	Length of pilot
τ_d	Length of downlink transmission
τ_c	Length of coherence interval
ρ_p	Normalized SNR related to pilot
ρ_d	Normalized SNR related to data signal
P_p	UE transmit power
P_d	transmit power of AP
σ^2	Noise variance
$\boldsymbol{\varphi}_k$	Pilot belonging to UE_k
$\kappa_{m,t}, \kappa_{m,r}$	Hardware quality with respect to AP_m
$\kappa_{k,t}, \kappa_{k,r}$	Hardware quality with respect to UE_k

that for a given power budget, the system with more RISs and fewer APs achieves a higher SE than the system with more APs and fewer RISs, resulting in a higher EE for the former. Therefore, it is preferred to deploy more RISs rather than APs to design a more cost-effective cell-free massive MIMO system.

C. Outline

The remaining of this paper is organized as follows. Section II introduces the cell-free massive MIMO system with RIS and describes the aggregated channel model. Section III gives the uplink training model with two channel estimation schemes in the presence of T-HWIs. Section IV derives closed-form SE expressions using the generic bounding technique and discusses several important observations. Section V validates the analytical results by simulations and Section VI concludes this paper.

D. Notations

We use lowercase and upper-case boldface letters to denote matrices and vectors. $\boldsymbol{A}^H$, $\boldsymbol{A}^T$, and $\boldsymbol{A}^*$ represent the conjugate transpose, the transpose, and the conjugate of matrix $\boldsymbol{A}$. Besides, $\mathbb{E}\{\boldsymbol{a}\}$, $\mathrm{diag}(\boldsymbol{a})$, $\|\boldsymbol{a}\|$, and $|a|$ are the expectation of vector $\boldsymbol{a}$, the diagonal matrix consisting of the diagonal entries of vector $\boldsymbol{a}$, the Euclid-norm of vector $\boldsymbol{a}$, and the modulus of scalar a, respectively. We have $\boldsymbol{A} \otimes \boldsymbol{B}$ to denote the Hadamard product of matrices $\boldsymbol{A}$ and $\boldsymbol{B}$. In addition, $\mathbb{C}^{N\times 1}$, $\boldsymbol{I}_N$, and $\boldsymbol{0}_N$ are the $N \times 1$ complex domain, the $N \times N$ identity matrix, and the $N \times 1$ zero vector. $\boldsymbol{n} \sim \mathcal{N}_{\mathbb{C}}(\boldsymbol{0}_N, \boldsymbol{I}_N)$ refers to a circularly symmetric complex Gaussian (CSCG) random vector with zero mean $\boldsymbol{0}_N$ and covariance matrix $\boldsymbol{I}_N$. Finally, we summarize the main notations in Sections II, III, and IV in TABLE I, shown at the top of this page.

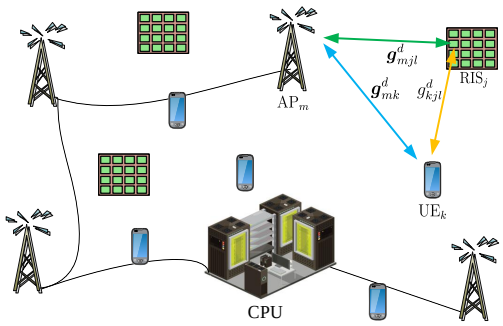

Fig. 1. An RIS-assisted cell-free massive MIMO system, where the aggregated channel between the AP and UE is the superposition of the direct and RIS-assisted indirect channels.

II. RIS-ASSISTED CELL-FREE MASSIVE MIMO MODEL

A downlink cell-free massive MIMO system with M N-antenna APs and K single-antenna UEs is considered, where all APs and UEs are equipped with low-quality hardware to alleviate the implementation cost and energy consumption. Besides, our system includes J RISs that are distributed according to a certain layout and each RIS possesses L scattering elements with individual control over the phase shifts of the incident signals, see Fig. 1. For the sake of brevity, we use $\mathrm{AP}_m, m \in \{1, 2, ..., M\}$, UE_k, $k \in \{1, 2, ..., K\}$, and RIS_{jl}, $j \in \{1, 2, ..., J\}, l \in \{1, 2, ..., L\}$ to denote the m-th AP, the k-th UE, and the l-th element of the j-th RIS, respectively. For analytical tractability, we consider an isotropic scattering environment and adopt the Rayleigh fading model [15] to characterize the channel responses among APs, UEs, and RISs. Then, the aggregate channel from AP_m to UE_k is given as

$$\boldsymbol{g}_{mk} = \boldsymbol{g}^d_{mk} + \sum_{j=1}^{J}\sum_{l=1}^{L} \boldsymbol{g}^c_{mkjl}, \tag{1}$$

where $\boldsymbol{g}^d_{mk} \sim \mathcal{N}_{\mathbb{C}}(\boldsymbol{0}_N, \beta^d_{mk}\boldsymbol{I}_N)$ is the direct channel from AP_m to UE_k with β^d_{mk} being the large-scale fading coefficient. Besides, $\boldsymbol{g}^c_{mkjl}$ refers to the cascaded channel between AP_m and UE_k via RIS_{jl}, which can be written as[1]

$$\boldsymbol{g}^c_{mkjl} = \boldsymbol{g}^d_{mjl} g^d_{kjl} f_{jl}, \tag{2}$$

where $\boldsymbol{g}^d_{mjl} \sim \mathcal{N}_{\mathbb{C}}(\boldsymbol{0}_N, \beta^d_{mj}\boldsymbol{I}_N)$ and $g^d_{kjl} \sim \mathcal{N}_{\mathbb{C}}\left(0, \beta^d_{kj}\right)$ are the channel responses from RIS_{jl} to AP_m and UE_k,

[1]We note that $\boldsymbol{g}^c_{mkjl}$ is the product of independent CSCG variables, implying that $\boldsymbol{g}^c_{mkjl}$ is generally not Gaussian distributed. Consequently, $\boldsymbol{g}_{mk}$ is also not Gaussian distributed.

respectively. Here, β_{mj}^{d} and β_{kj}^{d} correspond to the relevant large-scale fading coefficients. In addition, $f_{jl} = \alpha_{jl}e^{i\theta_{jl}}$ characterizes the frequency response of RIS_{jl}, where i is the imaginary unit, $\alpha_{jl} \in [0,1]$ means the amplitude reflection coefficient, and $\theta_{jl} \in [0, 2\pi]$ represents the induced phase shift. Akin to [15]–[19], we let $\alpha_{jl} = 1, \forall l$ to achieve the largest array gain and maximize the reflected signal when RIS_j is turned ON to reflect the pilot and payload data signals. In accordance with most works on RIS-assisted cell-free massive MIMO systems, our system is operated in time-division-duplex mode and each coherence interval is divided into two sub-intervals, i.e., one for uplink channel estimation and the other for downlink data transmission. In the following, the uplink training is detailed first.

III. Uplink Channel Estimation

Since the RIS lacks the active radio frequency chains and power amplifiers, the channel via RIS needs to be estimated through uplink training. To this end, we require the UEs to send the preassigned pilots to APs and then the APs use the linear minimum mean square error (LMMSE) estimate technique to estimate uplink CSI, which will be used to design the precoding matrices based on the channel reciprocity[2]. In the following, two LMMSE channel estimation schemes in the presence of T-HWIs are detailed.

A. Direct Estimation Scheme

We first focus on the DE scheme, a common approach for acquiring the uplink CSI in RIS-assisted cell-free massive MIMO systems [15]–[18]. This scheme enables a rough estimation of the aggregate channel $\boldsymbol{g}_{mk}$ with minimal pilot overhead. Let $\sqrt{\tau_p}\boldsymbol{\varphi}_k \in \mathbb{C}^{\tau_p \times 1}$ be the pilot belonging to UE_k with $\boldsymbol{\varphi}_k^H \boldsymbol{\varphi}_k = 1, \forall k$, where τ_p denotes the length of the pilot signal. To achieve a higher transmission efficiency, we assume that τ_p is much smaller than the length of the coherence interval τ_c, implying that K is usually larger than τ_p. In this case, different UEs inevitably share the same pilot, which gives rise to the pilot contamination [36]. We let $\mathcal{P}_k$ denote the set of UEs that reuse the same pilot as UE_k, including k itself. It is easy to obtain $\boldsymbol{\varphi}_k^H \boldsymbol{\varphi}_{k'} = 1,\ \forall k' \in \mathcal{P}_k$. Assuming all UEs transmit pilots with full power and modeling the T-HWIs according to the EVM [27]–[31], the received pilot signal at AP_m can be expressed as

$$\boldsymbol{Y}_{m,p} = \sqrt{\kappa_{m,r}} \left(\sum_{k=1}^{K} \boldsymbol{g}_{mk} \left(\sqrt{\tau_p \rho_p \kappa_{k,t}} \boldsymbol{\varphi}_k^H + \boldsymbol{\omega}_{k,t}^H \right) \right) + \boldsymbol{W}_{m,r} + \boldsymbol{N}_{m,p}, \tag{3}$$

where $\rho_p = \frac{P_p}{\sigma^2}$ is the normalized SNR of the pilot signal with P_p and σ^2 being the pilot transmit power and noise variance. $\boldsymbol{N}_{m,p}$ is the additive CSCG noise with the v-th column satisfying $\left[\boldsymbol{N}_{m,p}\right]_v \sim \mathcal{N}_{\mathbb{C}}\left(\boldsymbol{0}_N, \boldsymbol{I}_N\right)$, $\kappa_{m,r} \in [0,1]$ and $\kappa_{k,t} \in [0,1]$ refer to the linear hardware qualities related to AP_m and UE_k, respectively. $\boldsymbol{\omega}_{k,t} \in \mathbb{C}^{\tau_p \times 1}$ and $\boldsymbol{W}_{m,r} \in \mathbb{C}^{N \times \tau_p}$ characterize the additive HWIs of UE_k and AP_m, which can be modeled as

$$\boldsymbol{\omega}_{k,t} \sim \mathcal{N}_{\mathbb{C}}\left(\boldsymbol{0}_{\tau_p}, \rho_p\left(1-\kappa_{k,t}\right)\boldsymbol{I}_{\tau_p}\right), \tag{4}$$

$$\left[\mathbf{W}_{m,r}\right]_v \Big| \{\boldsymbol{g}_{mk}\} \sim \mathcal{N}_{\mathbb{C}}\Bigg(\boldsymbol{0}_N, \rho_p\left(1-\kappa_{m,r}\right) \times \sum_{k=1}^{K} \mathrm{diag}\left(\left|[\boldsymbol{g}_{mk}]_1\right|^2, ..., \left|[\boldsymbol{g}_{mk}]_N\right|^2\right)\Bigg), \tag{5}$$

where $\left[\boldsymbol{W}_{m,r}\right]_v$ means the v-th column of $\boldsymbol{W}_{m,r}$ and Eq. (5) is the conditional distribution given the set of $\{\boldsymbol{g}_{mk}\}$ in a coherence interval. Specifically, we can rewrite $\left[\boldsymbol{W}_{m,r}\right]_v$ as

$$\left[\boldsymbol{W}_{m,r}\right]_v = \sqrt{\rho_p\left(1-\kappa_{m,r}\right)} \sum_{k=1}^{K} \boldsymbol{g}_{mk} \otimes \boldsymbol{w}_{mk,rv}, \tag{6}$$

where $\boldsymbol{w}_{mk,rv} \sim \mathcal{N}_{\mathbb{C}}\left(\boldsymbol{0}_N, \boldsymbol{I}_N\right)$ is the CSCG variable. The above analysis shows that the impact of T-HWIs diminishes as the transceiver quality factor increases. In particular, $\kappa_{m,r} = \kappa_{k,t} = 1$ corresponds to the ideal hardware case while $\kappa_{m,r} = \kappa_{k,t} = 0$ implies the useless hardware case. Without loss of generality, we focus on estimating $\boldsymbol{g}_{mk}$, which requires projecting $\boldsymbol{Y}_{m,p}$ on $\boldsymbol{\varphi}_k$ and results in

$$\boldsymbol{y}_{mk,p} = \sqrt{\tau_p \rho_p \kappa_{m,r}} \sum_{k'=1}^{K} \sqrt{\kappa_{k',t}} \boldsymbol{g}_{mk'} \boldsymbol{\varphi}_{k'}^H \boldsymbol{\varphi}_k + \boldsymbol{N}_{m,p}\boldsymbol{\varphi}_k + \sqrt{\kappa_{m,r}} \sum_{k'=1}^{K} \boldsymbol{g}_{mk'} \boldsymbol{\omega}_{k',t}^H \boldsymbol{\varphi}_k + \boldsymbol{W}_{m,r}\boldsymbol{\varphi}_k. \tag{7}$$

Given Eq. (7), the LMMSE estimate of $\boldsymbol{g}_{mk}$ is presented in the following Lemma 1.

Lemma 1: Assuming that both APs and UEs are equipped with low-quality transceivers, the DE-based LMMSE estimate of the aggregated channel $\boldsymbol{g}_{mk}, \forall l, \forall k$ by resorting to the EVM model is formulated as

$$\hat{\boldsymbol{g}}_{mk}^{\mathrm{DE}} = \frac{\mathbb{E}\left\{\boldsymbol{g}_{mk}^H \boldsymbol{y}_{mk,p}\right\}}{\mathbb{E}\left\{\left\|\boldsymbol{y}_{mk,p}\right\|^2\right\}} \boldsymbol{y}_{mk,p} = c_{mk}^{\mathrm{DE}} \boldsymbol{y}_{mk,p}, \tag{8}$$

where

$$c_{mk}^{\mathrm{DE}} = \frac{\sqrt{\tau_p \rho_p \kappa_{m,r} \kappa_{k,t}} \beta_{mk}}{\tau_p \rho_p \kappa_{m,r} \sum\limits_{k' \in \mathcal{P}_k} \kappa_{k',t} \beta_{mk'} + \rho_p \sum\limits_{k'=1}^{K} \left(1 - \kappa_{m,r} \kappa_{k',t}\right) \beta_{mk'} + 1}, \tag{9}$$

and where $\beta_{mk} = \beta_{mk}^{d} + L\sum_{j=1}^{J} \beta_{mkj}^{c} = \beta_{mk}^{d} + L\sum_{j=1}^{J} \beta_{mj}^{d} \beta_{kj}^{d}$ is the sum of the large-scale fading coefficients of direct and indirect channels. Define $\boldsymbol{\varepsilon}_{mk}^{\mathrm{DE}} = \boldsymbol{g}_{mk} - \hat{\boldsymbol{g}}_{mk}^{\mathrm{DE}}$ as the channel estimation error under the DE scheme, the expectations of the norm squares of $\hat{\boldsymbol{g}}_{mk}^{\mathrm{DE}}$ and $\boldsymbol{\varepsilon}_{mk}^{\mathrm{DE}}$ are respectively expressed as

$$\mathbb{E}\left\{\left\|\hat{\boldsymbol{g}}_{mk}^{\mathrm{DE}}\right\|^2\right\} = N\gamma_{mk}^{\mathrm{DE}}, \mathbb{E}\left\{\left\|\boldsymbol{\varepsilon}_{mk}^{\mathrm{DE}}\right\|^2\right\} = N\left(\beta_{mk} - \gamma_{mk}^{\mathrm{DE}}\right), \tag{10}$$

where $\gamma_{mk}^{\mathrm{DE}} = \sqrt{\tau_p \rho_p \kappa_{m,r} \kappa_{k,t}} \beta_{mk} c_{mk}^{\mathrm{DE}}$.

Proof 1: See Appendix A.

[2]We use the LMMSE technique to estimate the aggregated channels by assuming the RIS phase shifts are constant within the training phase [16]–[18]. Although this technique may have a lower estimation accuracy than that of other known techniques [9] and [10], whereby the direct channels of the AP-RIS and RIS-UE links at specific time slots are separately estimated, the LMMSE technique facilitates the derivation of the closed-form expression of the SE performance metric. Moreover, the derived closed-form expression depends only on the large-scale fading coefficients rather than the small-scale fading coefficients, thus allowing for long-term optimization.

Remark 1: By comparing with [15, Eq. (4)] and [16, Eq. (15)], we notice that using low-quality hardware not only makes the numerator of $\gamma_{mk}^{\mathrm{DE}}$ correlate with $\kappa_{m,r}\kappa_{k,t}$, but also introduces a new inter-UE interference to the denominator of $\gamma_{mk}^{\mathrm{DE}}$, which implies that the use of low-quality hardware directly degrades $\gamma_{mk}^{\mathrm{DE}}$. Obviously, the lower the hardware quality, the worse the channel estimation. Furthermore, we can infer that the magnitude of the first term in the denominator of $\gamma_{mk}^{\mathrm{DE}}$ is strongly affected by the degree of the pilot contamination. Since the DE scheme cannot separate the direct and RIS-assisted indirect channels, it may result in poor channel estimation due to low estimation accuracy.

B. Modified ON/OFF Scheme

To improve the accuracy of the channel estimation, Bashar et al. [19] proposed an OE scheme, which divides the whole channel estimation phase into $1+JL$ sub-phases and estimates all direct and RIS-assisted indirect channels sequentially. However, it requires $(1+JL)\,\tau_p$ samples for channel estimation in each coherence interval, which incurs a high pilot overhead and reduces the transmission efficiency. In the following, our aim is to design a channel estimation scheme that balances the estimation accuracy and the pilot overhead. Specifically, our estimation scheme splits the whole channel estimation time into $1+J$ sub-phases.

1) 1st sub-phase: In this sub-phase, all scattering elements are OFF[3] and the UEs transmit pilots to the APs to estimate the direct channels from APs to UEs. Using the same estimate technique in Section III-A, the LMMSE estimate of $\boldsymbol{g}_{mk}^{d}, \forall m, \forall k$ is formulated as $\hat{\boldsymbol{g}}_{mk}^{d} = c_{mk}^{d}\boldsymbol{Y}_{m,p}^{d}\boldsymbol{\varphi}_k$, where

$$c_{mk}^{d} = \frac{\sqrt{\tau_p\rho_p\kappa_{m,r}\kappa_{k,t}}\beta_{mk}^{d}}{\tau_p\rho_p\kappa_{m,r}\sum\limits_{k'\in\mathcal{P}_k}\kappa_{k',t}\beta_{mk'}^{d}+\rho_p\sum\limits_{k'=1}^{K}\left(1-\kappa_{m,r}\kappa_{k',t}\right)\beta_{mk'}^{d}+1}, \tag{11}$$

and

$$\boldsymbol{Y}_{m,p}^{d} = \sqrt{\kappa_{m,r}}\left(\sum\nolimits_{k=1}^{K}\boldsymbol{g}_{mk}^{d}\left(\sqrt{\tau_p\rho_p\kappa_{k,t}}\boldsymbol{\varphi}_k^{H}+\boldsymbol{\omega}_{k,t}^{d}\right)\right) + \boldsymbol{W}_{m,r}^{d}+\boldsymbol{N}_{m,p}^{d}. \tag{12}$$

Note that in Eq. (12), $\boldsymbol{N}_{m,p}^{d}$, $\boldsymbol{\omega}_{k,t}^{d}$, and $\boldsymbol{W}_{m,r}^{d}$ are the CSCG noise, transmitter HWI, and receiver HWI within the 1st estimation sub-phase, which satisfy $\left[\boldsymbol{N}_{m,p}^{d}\right]_v \sim \mathcal{N}_{\mathbb{C}}\left(\boldsymbol{0}_N, \boldsymbol{I}_N\right)$, $\boldsymbol{\omega}_{k,t}^{d} \sim \mathcal{N}_{\mathbb{C}}\left(\boldsymbol{0}_{\tau_p}, \rho_p\left(1-\kappa_{k,t}\right)\boldsymbol{I}_{\tau_p}\right)$, and $\left[\boldsymbol{W}_{m,r}^{d}\right]_\tau \big| \{\boldsymbol{g}_{mk}\} \sim \mathcal{N}_{\mathbb{C}}\left(\boldsymbol{0}_N, \rho_p\left(1-\kappa_{m,r}\right)\sum_{k=1}^{K}\mathrm{diag}\left(\left|\left[\boldsymbol{g}_{mk}^{d}\right]_1\right|^2, ..., \left|\left[\boldsymbol{g}_{mk}^{d}\right]_N\right|^2\right)\right)$. Based on the above, we obtain $\mathbb{E}\left\{\left\|\hat{\boldsymbol{g}}_{mk}^{d}\right\|^2\right\} = N\gamma_{mk}^{d}$, where $\gamma_{mk}^{d} = \sqrt{\tau_p\rho_p\kappa_{m,r}\kappa_{k,t}}\beta_{mk}^{d}c_{mk}^{d}$.

2) $(j+1)$-th sub-phase: In this sub-phase, only the elements of RIS_j are ON and all other RIS elements are OFF. Define $\bar{\boldsymbol{g}}_{mkj}^{c} = \sum_{l=1}^{L}\boldsymbol{g}_{mkjl}^{c}$ as the sum of the cascaded channels from AP_m to UE_k via RIS_j, the received pilot signal at AP_m when all UEs simultaneously send pilots to the APs can be given as

$$\boldsymbol{Y}_{mj,p} = \sqrt{\kappa_{m,r}}\left(\sum\nolimits_{k=1}^{K}\left(\boldsymbol{g}_{mk}^{d}+\bar{\boldsymbol{g}}_{mkj}^{c}\right)\left(\sqrt{\tau_p\rho_p\kappa_{k,t}}\boldsymbol{\varphi}_k^{H} + \left(\boldsymbol{\omega}_{kj,t}^{c}\right)^{H}\right)\right) + \boldsymbol{W}_{mj,r}^{c}+\boldsymbol{N}_{mj,p}^{c}, \tag{13}$$

where $\boldsymbol{W}_{mj,r}$ and $\boldsymbol{N}_{mj,p}$ are the receiver HWI and CSCG white noise within the $(j+1)$-th channel estimation sub-phase. Since $\boldsymbol{Y}_{m,p}^{d}$ is known at AP_m and $\boldsymbol{Y}_{mj,p}$ actually contains $\boldsymbol{Y}_{m,p}^{d}$, we can subtract it from $\boldsymbol{Y}_{mj,p}$, which leads to

$$\boldsymbol{Y}_{mj,p}^{c} = \sqrt{\kappa_{m,r}}\left(\sum_{k=1}^{K}\bar{\boldsymbol{g}}_{mkj}^{c}\left(\sqrt{\tau_p\rho_p\kappa_{k,t}}\boldsymbol{\varphi}_k^{H}+\left(\boldsymbol{\omega}_{kj,t}^{c}\right)^{H}\right)\right) + \boldsymbol{W}_{mj,r}^{c}+\boldsymbol{N}_{mj,p}^{c}, \tag{14}$$

where $\left[\boldsymbol{N}_{mj,p}^{c}\right]_v \sim \mathcal{N}_{\mathbb{C}}\left(\boldsymbol{0}_N, \boldsymbol{I}_N\right)$ and $\left[\boldsymbol{W}_{mj,r}^{c}\right]_v \big| \{\bar{\boldsymbol{g}}_{mkj}^{c}\} \sim \mathcal{N}_{\mathbb{C}}\left(\boldsymbol{0}_N, \rho_p\left(1-\kappa_{m,r}\right)\sum_{k=1}^{K}\mathrm{diag}\left(\left|\left[\bar{\boldsymbol{g}}_{mkj}^{c}\right]_1\right|^2, ..., \left|\left[\bar{\boldsymbol{g}}_{mkj}^{c}\right]_N\right|^2\right)\right)$. The projection of $\boldsymbol{Y}_{mj,p}^{c}$ on $\boldsymbol{\varphi}_k$ is equal to

$$\boldsymbol{y}_{mkj,p}^{c} = \sqrt{\tau_p\rho_p\kappa_{m,r}}\sum_{k'=1}^{K}\sqrt{\kappa_{k',t}}\bar{\boldsymbol{g}}_{mk'j}^{c}\boldsymbol{\varphi}_{k'}^{H}\boldsymbol{\varphi}_k + \boldsymbol{N}_{mj,p}^{c}\boldsymbol{\varphi}_k + \sqrt{\kappa_{m,r}}\sum_{k'=1}^{K}\bar{\boldsymbol{g}}_{mk'j}^{c}\left(\boldsymbol{\omega}_{k'j,t}^{c}\right)^{H}\boldsymbol{\varphi}_k + \boldsymbol{W}_{mj,r}^{c}\boldsymbol{\varphi}_k. \tag{15}$$

Given $\boldsymbol{y}_{mkj,p}^{c}$, the LMMSE of $\boldsymbol{g}_{mkj}^{c}$ is expressed as $\hat{\boldsymbol{g}}_{mkj}^{c} = c_{mkj}^{c}\boldsymbol{y}_{mkj,p}^{c}$, where

$$c_{mkj}^{c} = \frac{L\sqrt{\tau_p\rho_p\kappa_{m,r}\kappa_{k,t}}\beta_{mkj}^{c}}{L\tau_p\rho_p\kappa_{m,r}\sum\limits_{k'\in\mathcal{P}_k}\kappa_{k',t}\beta_{mk'j}^{c}+L\rho_p\sum\limits_{k'=1}^{K}\left(1-\kappa_{m,r}\kappa_{k',t}\right)\beta_{mk'j}^{c}+1}. \tag{16}$$

Besides, the expectation of the norm square of $\hat{\boldsymbol{g}}_{mkj}^{c}$ is $\mathbb{E}\left\{\left\|\hat{\boldsymbol{g}}_{mkj}^{c}\right\|^2\right\} = N\gamma_{mkj}^{c}$, where $\gamma_{mkj}^{c} = L\sqrt{\tau_p\rho_p\kappa_{m,r}\kappa_{k,t}}\times\beta_{mkj}^{c}c_{mkj}^{c}$.

Based on the above, the LMMSE estimate of $\boldsymbol{g}_{mk}, \forall l, \forall k$ under the MOE scheme is established in the following Lemma.

Lemma 2: Assuming the APs and UEs are equipped with low-quality transceivers, the MOE-based LMMSE estimate of the aggregated channel $\boldsymbol{g}_{mk}, \forall l, \forall k$ by resorting to the EVM model is formulated as

$$\hat{\boldsymbol{g}}_{mk}^{\mathrm{MOE}} = \hat{\boldsymbol{g}}_{mk}^{d}+\sum_{j=1}^{J}\hat{\boldsymbol{g}}_{mkj}^{c} = c_{mk}^{d}\boldsymbol{y}_{mk,p}^{d}+\sum_{j=1}^{J}c_{mkj}^{c}\boldsymbol{y}_{mkj,p}^{c}. \tag{17}$$

Define $\boldsymbol{\varepsilon}_{mk}^{\mathrm{MOE}} = \boldsymbol{g}_{mk}-\hat{\boldsymbol{g}}_{mk}^{\mathrm{MOE}}$ as the channel estimation error associated with the MOE scheme, the expectations of the norm squares of $\hat{\boldsymbol{g}}_{mk}^{\mathrm{MOE}}$ and $\boldsymbol{\varepsilon}_{mk}^{\mathrm{MOE}}$ are respectively expressed as

$$\mathbb{E}\left\{\left\|\hat{\boldsymbol{g}}_{mk}^{\mathrm{MOE}}\right\|^2\right\} = N\gamma_{mk}^{\mathrm{MOE}},\ \mathbb{E}\left\{\left\|\boldsymbol{\varepsilon}_{mk}^{\mathrm{MOE}}\right\|^2\right\} = N\left(\beta_{mk}-\gamma_{mk}^{\mathrm{MOE}}\right), \tag{18}$$

where $\gamma_{mk}^{\mathrm{MOE}} = \gamma_{mk}^{d}+\sum_{j=1}^{J}\gamma_{mkj}^{c}$.

Proof 2: The estimation of the aggregated channel can be regarded as the sum of the estimations of the direct channel and indirect RIS-assisted channels. Therefore, Lemma 2 can

[3]We note that it is difficult to turn off an RIS and thereby remove it from the propagation model since the surface will still be there and influence the propagation environment. To implement the MOE scheme, we assume that the RIS elements that are not involved in a considered training sub-phase, i.e., $\mathrm{RIS}_{j'}, \forall j' \neq j$, are set to appropriate magnitude values such that their combined channel effect is negligible [37], [38]. It is out of the scope of this work to investigate how to choose these values and we assume that they are known in advance.

be proved by combining the results in Eqs. (11), (12), (15), and (16).

Remark 2: Lemma 2 shows that the MOE-based channel estimation has common and distinct features with the DE-based channel estimation in Lemma 1. It is evident that the MOE scheme is sensitive to the hardware quality because $\gamma_{mk}^{\mathrm{MOE}}$ acts as a decreasing function with respect to the hardware quality. Moreover, $\hat{\boldsymbol{g}}_{mk}^{\mathrm{MOE}}$ does not follow a Gaussian distribution in general, because it depends on $\boldsymbol{y}_{mk,p}^{d}$ and $\boldsymbol{y}_{mkj,p}^{c}$, which are products of independent CSCG variables. The advantage of the MOE scheme over the DE scheme is its higher channel estimation accuracy, which can be quantified by the NMSE-CE metrics presented below.

According to [39] and [40], the NMSEs-CE for both DE and MOE schemes can be respectively defined as

$$\mathcal{E}_N^{\mathrm{DE}} = \frac{\sum\limits_{m,k} \mathbb{E}\left\{\left\|\boldsymbol{\epsilon}_{mk}^{\mathrm{DE}}\right\|^2\right\}}{\sum\limits_{m,k} \mathbb{E}\left\{\left\|\boldsymbol{g}_{mk}\right\|^2\right\}} = \frac{\sum\limits_{m,k}\left(\beta_{mk}-\gamma_{mk}^{\mathrm{DE}}\right)}{\sum\limits_{m,k}\beta_{mk}}, \tag{19}$$

and

$$\mathcal{E}_N^{\mathrm{MOE}} = \frac{\sum\limits_{m,k} \mathbb{E}\left\{\left\|\boldsymbol{\epsilon}_{mk}^{\mathrm{MOE}}\right\|^2\right\}}{\sum\limits_{m,k} \mathbb{E}\left\{\left\|\boldsymbol{g}_{mk}\right\|^2\right\}} = \frac{\sum\limits_{m,k}\left(\beta_{mk}-\gamma_{mk}^{\mathrm{MOE}}\right)}{\sum\limits_{m,k}\beta_{mk}}. \tag{20}$$

Recalling that $\gamma_{mk}^{\mathrm{DE}}$ and $\gamma_{mk}^{\mathrm{MOE}}$ are linear-fractional functions with respect to ρ_p, if we let $\rho_p \to \infty$, i.e., a high SNR regime is considered, $\mathcal{E}_N^{\mathrm{DE}}$ and $\mathcal{E}_N^{\mathrm{MOE}}$ approach to

$$\lim_{\rho_p\to\infty} \mathcal{E}_N^{\mathrm{DE}} = \frac{\sum\limits_{m,k}\left(\beta_{mk} - \dfrac{\left(\beta_{mk}\right)^2}{\sum\limits_{k'\in\mathcal{P}_k}\frac{\kappa_{k',t}}{\kappa_{k,t}}\beta_{mk'} + \sum\limits_{k'=1}^{K}\frac{1-\kappa_{m,r}\kappa_{k',t}}{\tau_p\kappa_{m,r}\kappa_{k,t}}\beta_{mk'}}\right)}{\sum\limits_{m,k}\beta_{mk}}, \tag{21}$$

and

$$\begin{aligned}\lim_{\rho_p\to\infty} \mathcal{E}_N^{\mathrm{MOE}} =& \frac{\sum\limits_{m,k}\beta_{mk} - \sum\limits_{m,k}\dfrac{\left(\beta_{mk}^{d}\right)^2}{\sum\limits_{k'\in\mathcal{P}_k}\frac{\kappa_{k',t}}{\kappa_{k,t}}\beta_{mk'}^{d} + \sum\limits_{k'=1}^{K}\frac{1-\kappa_{m,r}\kappa_{k',t}}{\tau_p\kappa_{m,r}\kappa_{k,t}}\beta_{mk'}^{d}}}{\sum\limits_{m,k}\beta_{mk}} \\ &- \frac{\sum\limits_{m,k,j}\dfrac{L\left(\beta_{mkj}^{c}\right)^2}{\sum\limits_{k'\in\mathcal{P}_k}\frac{\kappa_{k',t}}{\kappa_{k,t}}\beta_{mk'j}^{c} + \sum\limits_{k'=1}^{K}\frac{1-\kappa_{m,r}\kappa_{k',t}}{\tau_p\kappa_{m,r}\kappa_{k,t}}\beta_{mk'j}^{c}}}{\sum\limits_{m,k}\beta_{mk}}.\end{aligned} \tag{22}$$

Remark 3: The numerators in Eqs. (21) and (22) determine the channel estimation error-floors, which are functions of the hardware quality, length of the pilot signal, number of RISs, and number of elements per RIS. It is clear that we can reduce $\mathcal{E}_N^{\mathrm{DE}}$ and $\mathcal{E}_N^{\mathrm{MOE}}$ by using more orthogonal pilots and increasing the hardware quality. However, as long as the pilot contamination or T-HWI exists, both $\mathcal{E}_N^{\mathrm{DE}}$ and $\mathcal{E}_N^{\mathrm{MOE}}$ cannot approach 0 even ρ_p grows to infinity and there will always be non-zero lower bounds. In general, $\mathcal{E}_N^{\mathrm{MOE}}$ is lower than $\mathcal{E}_N^{\mathrm{DE}}$ because it estimates the direct and indirect RIS-assisted channels separately. However, in the ideal hardware case without pilot contamination, $\mathcal{E}_N^{\mathrm{MOE}}$ may be higher than $\mathcal{E}_N^{\mathrm{DE}}$ due to the small path gain of $\boldsymbol{g}_{mkjl}^{c}$ compared to $\boldsymbol{g}_{mk}^{d}$. This will be further discussed in Section V.

IV. Downlink Data Transmission

After estimating the uplink CSI, the APs start to transmit data signal to the UEs within the remaining τ_d samples of each coherence interval. Thanks to the channel reciprocity, the APs can use the estimated uplink CSI as the downlink counterpart and precode the signal intended for the UEs. Let s_k denote the data signal for UE_k, where $\mathbb{E}\{s_k s_{k'}^*\} = 1$, if $k = k'$ and 0 otherwise, then the data signal transmitted from AP_m with HWIs can be expressed as

$$\boldsymbol{t}_m = \sqrt{\rho_d \kappa_{m,t}} \sum_{k'=1}^{K} \sqrt{\eta_{mk'}^{X}} \left(\hat{\boldsymbol{g}}_{mk'}^{X}\right)^* s_{k'} + \boldsymbol{\omega}_{m,t}^*, \tag{23}$$

where $\rho_d = \frac{P_d}{\sigma^2}$ denotes the normalized SNR related to the data signal with P_d being the data transmit power, $\kappa_{m,t} \in [0,1]$ is the hardware quality of AP_m, $\eta_{mk}^{X} \geqslant 0$ indicates the power control coefficient of AP_m for serving UE_k, $\left(\hat{\boldsymbol{g}}_{mk}^{X}\right)^*$ is the conjugate beamforming matrix depending on the estimated uplink CSI with $X \in \{\mathrm{DE}, \mathrm{MOE}\}$, and $\boldsymbol{\omega}_{m,t}^*$ represents the HWI of AP_m, which is expressed as

$$\boldsymbol{\omega}_{m,t}^* \sim \mathcal{N}_{\mathbb{C}}\left(\boldsymbol{0}_N, \rho_d\left(1-\kappa_{m,t}\right)\sum_{k'=1}^{K}\eta_{mk'}^{X}\gamma_{mk'}^{X}\boldsymbol{I}_N\right). \tag{24}$$

Note that in Eq. (24), $\gamma_{mk'}^{X}$ is the channel estimation quality with $X \in \{\mathrm{DE}, \mathrm{MOE}\}$. Based on Eq. (23), the data signal received at UE_k resulting from the joint coherent transmission by all APs can be written as

$$\begin{aligned}\hat{s}_k &= \sqrt{\kappa_{k,r}}\sum_{m=1}^{M}\boldsymbol{g}_{mk}^{T}\boldsymbol{t}_m + w_{k,r} + n_k \\ &= \sqrt{\rho_d\kappa_{k,r}}\sum_{k'=1}^{K}\sum_{m=1}^{M}\sqrt{\eta_{mk'}^{X}\kappa_{m,t}}\boldsymbol{g}_{mk}^{T}\left(\hat{\boldsymbol{g}}_{mk'}^{X}\right)^* s_{k'} \\ &\quad + \sqrt{\kappa_{k,r}}\sum_{m=1}^{M}\boldsymbol{g}_{mk}^{T}\boldsymbol{\omega}_{m,t}^* + w_{k,r} + n_k,\end{aligned} \tag{25}$$

where $\kappa_{k,r}$ is the hardware quality of UE_k, $n_k \sim \mathcal{N}_{\mathbb{C}}(0,1)$ is the CSCG white noise, and $w_{k,r}$ refers to the HWI of UE_k. According to [29], $w_{k,r}$ satisfies

$$w_{k,r} \sim \mathcal{N}_{\mathbb{C}}\left(0, \rho_d\left(1-\kappa_{k,r}\right)\sum_{m,k'}\eta_{mk'}^{X}\left|\boldsymbol{g}_{mk}^{T}\left(\hat{\boldsymbol{g}}_{mk'}^{X}\right)^*\right|^2\right). \tag{26}$$

Then, s_k can be detected from $\hat{s}_k$. To this end, we first rewrite Eq. (25) by virtue of the use-and-then-forget technique [1], as

$$\hat{s}_k = \mathrm{DS}_k \cdot s_k + \mathrm{BU}_k \cdot s_k + \mathrm{IUI}_{k'k} \cdot s_{k'} + \mathrm{THI}_k + w_{k,r} + n_k, \tag{27}$$

where

$$\mathrm{DS}_k = \sqrt{\rho_d\kappa_{k,r}}\sum_{m=1}^{M}\sqrt{\eta_{mk}^{X}\kappa_{m,t}}\mathbb{E}\left\{\boldsymbol{g}_{mk}^{T}\left(\hat{\boldsymbol{g}}_{mk}^{X}\right)^*\right\}, \tag{28}$$

$$\mathrm{BU}_k = \sqrt{\rho_d\kappa_{k,r}}\sum_{m=1}^{M}\sqrt{\eta_{mk}^{X}\kappa_{m,t}}\left(\boldsymbol{g}_{mk}^{T}\left(\hat{\boldsymbol{g}}_{mk}^{X}\right)^* - \mathbb{E}\left\{\boldsymbol{g}_{mk}^{T}\left(\hat{\boldsymbol{g}}_{mk}^{X}\right)^*\right\}\right), \tag{29}$$

$$\mathrm{IUI}_{k'k} = \sqrt{\rho_d \kappa_{k,r}} \sum_{m=1}^{M} \sqrt{\eta_{mk'}^{X} \kappa_{m,t}} \boldsymbol{g}_{mk}^{T} \left(\hat{\boldsymbol{g}}_{mk'}^{X} \right)^{*}, \quad (30)$$

and

$$\mathrm{THI}_k = \sqrt{\kappa_{k,r}} \sum_{m=1}^{M} \boldsymbol{g}_{mk}^{T} \boldsymbol{\omega}_{m,t}^{*}. \quad (31)$$

Note that the terms on the right-hand side of Eq. (27) are the desired signal, beamforming gain uncertainty, inter-UE interference, transmitter HWI, receiver HWI, and CSCG white noise, respectively. We can directly prove that these terms are pair-wisely uncorrelated with each other. Next, due to the uncorrelated Gaussian noise leads to the worst SE [41], a lower-bound for the downlink SE of RIS-assisted cell-free massive MIMO system with T-HWIs is given as

$$\mathcal{S}_k = B \frac{\tau_d}{\tau_c} \log_2 \left(1 + \frac{\mathbb{E}\{|\mathrm{DS}_k|^2\}}{\mathbb{E}\{|\mathrm{BU}_k|^2\} + \sum\limits_{k' \neq k}^{K} \mathbb{E}\{|\mathrm{IUI}_{k'k}|^2\} + \mathbb{E}\{|\mathrm{THI}_k|^2\} + \mathbb{E}\{|w_{k,r}|^2\} + 1} \right), \quad (32)$$

where B is the bandwidth and $\frac{\tau_d}{\tau_c}$ denotes the transmission efficiency. By calculating all expectations in Eq. (32), we obtain the following Theorem 1.

Theorem 1: Assuming the APs and UEs are equipped with low-quality transceivers, a downlink achievable SE of UE_k for the RIS-assisted cell-free massive MIMO system with the conjugate beamforming technique depending on specific channel estimation strategies is formulated as

$$\mathcal{S}_k^{X} = B \frac{\tau_d^{X}}{\tau_c} \log_2 \left(1 + \frac{N^2 \rho_d \kappa_{k,r} \left(\sum\limits_{m=1}^{M} \sqrt{\eta_{mk}^{X} \kappa_{m,t}} \bar{\mu}_{mkk}^{X} \right)^2}{D_{1k} + D_{2k} + D_{3k} + D_{4k} + D_{5k} + 1} \right), \quad (33)$$

where

$$D_{1k} = N \rho_d \sum_{k'=1}^{K} \sum_{m=1}^{M} \eta_{mk'}^{X} \beta_{mk} \bar{\mu}_{mk'k'}^{X}, \quad (34)$$

$$\begin{aligned} D_{2k} = {} & N^2 \rho_d \kappa_{k,r} \frac{1-\kappa_{k,t}}{\tau_p \kappa_{k,t}} \sum_{m=1}^{M} \sum_{m'=1}^{M} \sqrt{\eta_{mk}^{X} \eta_{m'k}^{X} \kappa_{m,t} \kappa_{m',t}} \bar{\gamma}_{mm'k}^{X} \\ & + N^2 \rho_d \left(1 - \kappa_{k,r}\right) \sum_{k'=1}^{K} \left(\left| \boldsymbol{\varphi}_{k'}^{H} \boldsymbol{\varphi}_k \right|^2 + \frac{1-\kappa_{k,t}}{\tau_p \kappa_{k,t}} \right) \sum_{m=1}^{M} \eta_{mk'}^{X} \left(\bar{\mu}_{mkk'}^{X} \right)^2 \\ & + N^2 \rho_d \kappa_{k,r} \sum_{k' \neq k}^{K} \left(\left| \boldsymbol{\varphi}_{k'}^{H} \boldsymbol{\varphi}_k \right|^2 + \frac{1-\kappa_{k,t}}{\tau_p \kappa_{k,t}} \right) \left(\sum_{m=1}^{M} \sqrt{\eta_{mk'}^{X} \kappa_{m,t}} \bar{\mu}_{mk'k'}^{X} \right)^2 \\ & + N \rho_d \rho_p \sum_{k'=1}^{K} \sum_{m=1}^{M} \eta_{mk'}^{X} \left(1 - \kappa_{m,r}\right) \left(\kappa_{k,r} \kappa_{m,t} + 1 - \kappa_{k,r} \right) \bar{\psi}_{mkk'}^{X}, \end{aligned} \quad (35)$$

$$\begin{aligned} D_{3k} = {} & N L \rho_d \rho_p \sum_{k'=1}^{K} \sum_{m=1}^{M} \eta_{mk'}^{X} \left(\kappa_{k,r} \kappa_{m,t} + 1 - \kappa_{k,r} \right) \\ & \times \left(\tau_p \kappa_{k,t} \kappa_{m,r} \left| \boldsymbol{\varphi}_{k'}^{H} \boldsymbol{\varphi}_k \right|^2 + 1 - \kappa_{k,t} \kappa_{m,r} \right) \sum_{j=1}^{J} \left(\bar{c}_{mk'j}^{X} \right)^2 \beta_{mkj}^2, \end{aligned} \quad (36)$$

$$\begin{aligned} D_{4k} = {} & N L \rho_d \rho_p \sum_{k'=1}^{K} \sum_{k''=1}^{K} \sum_{m=1}^{M} \eta_{mk'}^{X} \Big(\left(\kappa_{k,r} \kappa_{m,t} + 1 - \kappa_{k,r} \right) \left(1 - \kappa_{m,r}\right) \\ & + N \kappa_{m,r} \left(1 - \kappa_{k,r}\right) \left(\tau_p \kappa_{k'',t} \left| \boldsymbol{\varphi}_{k}^{H} \boldsymbol{\varphi}_k \right|^2 + 1 - \kappa_{k'',t} \right) \Big) \sum_{j=1}^{J} \left(\bar{c}_{mk'j}^{X} \right)^2 \beta_{mkj} \beta_{mk''j}, \end{aligned} \quad (37)$$

$$\begin{aligned} D_{5k} = {} & N^2 L \rho_d \rho_p \kappa_{k,r} \sum_{k'=1}^{K} \sum_{k''=1}^{K} \left(\tau_p \kappa_{k'',t} \left| \boldsymbol{\varphi}_{k''}^{H} \boldsymbol{\varphi}_{k'} \right|^2 + 1 - \kappa_{k'',t} \right) \\ & \times \sum_{m=1}^{M} \sum_{m'=1}^{M} \sqrt{\kappa_{m,r} \kappa_{m',r} \kappa_{m,t} \kappa_{m',t} \eta_{mk'}^{X} \eta_{m'k'}^{X}} \sum_{j=1}^{J} \bar{c}_{mk'j}^{X} \bar{c}_{m'k'j}^{X} \beta_{mkj} \beta_{m'k''j}, \end{aligned} \quad (38)$$

where $X \in \{\mathrm{DE}, \mathrm{MOE}\}$, $\tau_d^{\mathrm{DE}} = \tau_c - \tau_p$, $\bar{\mu}_{mkk'}^{\mathrm{DE}} = \gamma_{mk'}^{\mathrm{DE}} \frac{\beta_{mk}}{\beta_{mk'}}$, $\bar{\gamma}_{mm'k}^{\mathrm{DE}} = \gamma_{mk}^{\mathrm{DE}} \gamma_{m'k}^{\mathrm{DE}}$, $\bar{c}_{mkj}^{\mathrm{DE}} = c_{mk}^{\mathrm{DE}}$, $\bar{\psi}_{mkk'}^{\mathrm{DE}} = \left(c_{mk'}^{\mathrm{DE}} \beta_{mk} \right)^2$, $\tau_d^{\mathrm{MOE}} = \tau_c - (J+1)\tau_p$, $\bar{\mu}_{mkk'}^{\mathrm{MOE}} = \gamma_{mk'}^{d} \frac{\beta_{mk}^{d}}{\beta_{mk'}^{d}} + \sum_{j=1}^{J} \gamma_{mjk'}^{c} \frac{\beta_{mkj}^{c}}{\beta_{mk'j}^{c}}$, $\bar{\gamma}_{mm'k}^{\mathrm{MOE}} = \gamma_{mk}^{d} \gamma_{m'k}^{d} + \sum_{j=1}^{J} \gamma_{mjk}^{c} \gamma_{m'jk}^{c}$, $\bar{c}_{mkj}^{\mathrm{MOE}} = c_{mkj}^{c}$, $\bar{\psi}_{mkk'}^{\mathrm{MOE}} = \left(c_{mk'}^{d} \beta_{mk}^{d} \right)^2 + L^2 \sum_{j=1}^{J} \left(c_{mk'j}^{c} \beta_{mkj}^{c} \right)^2$.

Proof 3: Please see Appendix B.

Based on Eq. (33), the sum-SE of the RIS-assisted cell-free massive MIMO downlink system with T-HWIs is $\mathcal{S}_{sum}^{X} = \sum_{k=1}^{K} \mathcal{S}_k^{X}$.

Remark 4: Theorem 1 leads to the following observations on the RIS-assisted downlink SE.

1) The RIS-assisted downlink SE has some common and distinct features with the downlink SE without RIS [27]. As in [27, Eq. (21)], the desired signal power is proportional to $M^2 N^2$ or $\kappa_{k,r} \kappa_{m,t}$. However, there are also several interference terms that are either proportional to MN or independent of $\kappa_{k,r} \kappa_{m,t}$, implying that $\mathcal{S}_{sum}^{X}$ increases monotonically with respect to M, N, $\kappa_{k,r}$, and $\kappa_{m,t}$. Furthermore, a larger $\kappa_{m,r}$ or $\kappa_{k,t}$ results in a larger γ_{mk}^{X}, which improves $\mathcal{S}_{sum}^{X}$. Moreover, $\mathcal{S}_{sum}^{X}$ is more complex than [27, Eq. (21)] and it contains some new interference terms that arise from the correlation between the direct and indirect channels. Nevertheless, this does not mean that the use of RIS degrades the SE performance.

2) Focusing on $\mathcal{S}_{sum}^{X}$, it shows that the MOE scheme has a lower transmission efficiency than the DE scheme by a factor of $\frac{\tau_d^{\mathrm{MOE}}}{\tau_d^{\mathrm{DE}}} = \frac{\tau_c - (J+1)\tau_p}{\tau_c - \tau_p}$, which means that the MOE scheme sacrifices some transmission efficiency that increases with the number of RISs. However, the additional estimation accuracy gain offered by the MOE scheme can compensate this performance loss, especially in scenarios with non-ideal hardware and severe pilot contamination.

3) Theorem 1 indicates that under Rayleigh fading channels, the RIS phase shifts do not affect $\mathcal{S}_{sum}^{X}$. It is consistent with Lemmas 1 and 2, where the LMMSE-based channel estimations are also independent of the RIS phase shifts. Consequently, this work does not consider the phase optimization strategy. The derived SE expression makes a preliminary contribution to analyze the downlink performance of an RIS-assisted cell-free massive MIMO system with T-HWIs under both DE and MOE schemes, and can be reasonably regarded as a lower bound to the RIS-assisted cell-free performance metric.

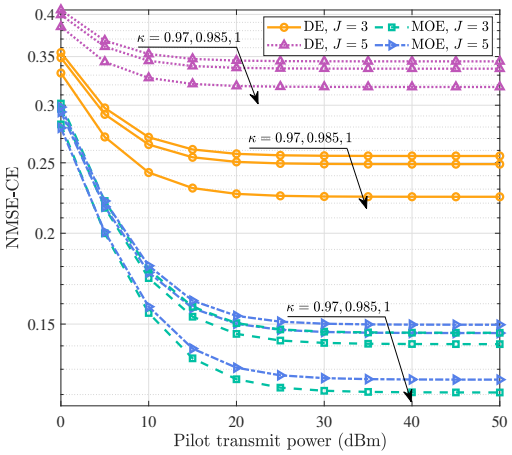

Fig. 2. NMSE-CEs of DE and MOE schemes versus the transmit power of pilot under different degrees of T-HWIs and numbers of RISs. Here, $M=50$, $K=10$, $N=2$, $L=500$, and $\tau_p=2$.

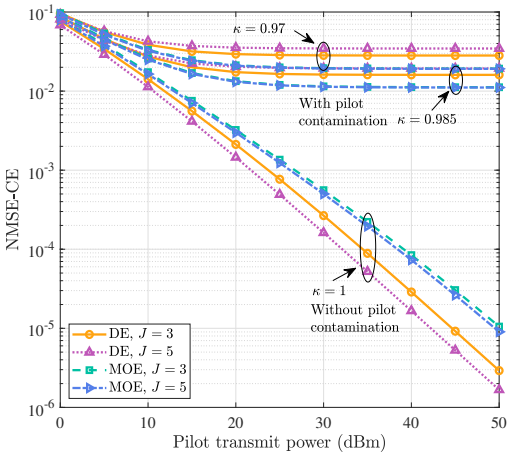

Fig. 3. NMSE-CEs of DE and MOE schemes versus the transmit power of pilot under different degrees of T-HWIs and numbers of RISs. Here, $M=50$, $K=10$, $N=2$, $L=500$, and $\tau_p=10$.

V. Simulation Results And Performance Analysis

This section presents experimental simulations to validate the theoretical analysis in Sections III and IV and compare the performance of hardware-impaired cell-free massive MIMO systems with and without RIS under various system settings (such as different hardware quality, numbers of APs/UEs/RISs/elements per RIS, transmit power of AP/UE, RIS layout, etc.).

The considered system consists of M APs, K UEs, J RISs, and one CPU. The communication region is a square of size $D\times D$ with $D=1.5$ km and the four vertices of the considered region are $\left(\frac{-D}{2},\frac{D}{2}\right)$ km, $\left(\frac{-D}{2},\frac{-D}{2}\right)$ km, $\left(\frac{D}{2},\frac{-D}{2}\right)$ km, and $\left(\frac{D}{2},\frac{D}{2}\right)$ km, respectively, where the coordinate $(x,\ y)$ denotes the two-dimensional location. Similar to [16] and [18], all APs are randomly distributed in the sub-region of $x^{\text{AP}},y^{\text{AP}}\in\left[\frac{-D}{2},\frac{-D}{3}\right]$ km and all UEs are randomly scattered in the sub-region of $x^{\text{UE}},y^{\text{UE}}\in\left[\frac{D}{4},\frac{D}{3}\right]$ km. Besides, we start by assuming that all RISs are randomly placed near the UEs with coordinates $\left(x^{\text{UE}}\pm\frac{D}{150},y^{\text{UE}}\pm\frac{D}{150}\right)$. The large-scale fading coefficients of the direct channels from AP_m to UE_k, AP_m to RIS_j, and UE_k to RIS_j are modeled by $\beta^d_{mk}=\text{PL}_{mk}z_{mk}$, $\beta^d_{mj}=\text{PL}_{mj}z_{mj}$, and $\beta^d_{kj}=\text{PL}_{kj}z_{kj}$, where PL_{mk}, PL_{mj}, and PL_{kj} represent the path-loss coefficients according to the three-slope path-loss model [1, Eq. (52)] and $z_{mk},z_{mj},z_{jk}\sim\mathcal{N}_{\mathbb{C}}\left(0,\sigma_{sh}\right)$ capture the shadow fading with $\sigma_{sh}=8$ dB being the standard deviation. The heights of the AP, UE, and RIS are set as 15 m, 1.65 m, and 30 m. Each coherence interval consists of $\tau_c=200$ samples and the bandwidth B is equal to 20 MHz. We assume that each AP or UE has the same transceiver quality during the training and data transmission phases and let $\kappa_{m,AP}$ and $\kappa_{k,UE}$ denote the quality factors of AP_m and UE_k. Moreover, we set $P_p=100$ mW, $P_d=200$ mW, $\sigma^2=-126$ dBm, and advocate the full power control strategy for simulation. Specifically, all APs transmit at their maximum power and the power coefficients of each AP for serving various UEs are the same, which leads to $\eta^{\text{DE}}_{mk}=\frac{1}{N\kappa_{m,t}\sum_{k'=1}^{K}\gamma^{\text{DE}}_{mk}}$, $\eta^{\text{MOE}}_{mk}=\frac{1}{N\kappa_{m,t}\sum_{k'=1}^{K}\gamma^{\text{MOE}}_{mk}},\forall m,\forall k$.

A. NMSE-CE Comparison Between DE and MOE Schemes

First of all, Fig. 2 illustrates the NMSE-CEs of the DE and MOE schemes $\mathcal{E}_N^{\text{DE}}$ and $\mathcal{E}_N^{\text{MOE}}$ versus the training power P_p under different degrees of T-HWIs and numbers of RISs, assuming $\kappa_{m,AP}=\kappa_{k,UE}=\kappa,\ \forall m,\ \forall k$. In Fig. 2, we set $\tau_p=2$ and $K=10$ to simulate a scenario with severe pilot contamination. It can be seen that the NMSE-CEs decrease with κ and have non-zero error-floors in the high P_p regime, regardless of the channel estimation scheme. This indicates that indefinitely increasing P_p cannot eliminate the channel estimation error-floors in the presence of pilot contamination. Furthermore, the MOE scheme has a lower NMSE-CE than the DE scheme, but its performance deteriorates with the number of RISs. This is because the MOE scheme requires $J+1$ rounds of channel estimation and the errors in each round are consistently accumulated.

Fig. 3 shows $\mathcal{E}_N^{\text{DE}}$ and $\mathcal{E}_N^{\text{MOE}}$ versus P_p under different degrees of T-HWIs and numbers of RISs without pilot contamination, using the same settings as in Fig. 2 except $\tau_p=10$. The error-floors are still present and $\mathcal{E}_N^{\text{DE}}$ is higher than $\mathcal{E}_N^{\text{MOE}}$ when non-ideal hardware is used. Only when sufficient pilots and ideal hardware are available, both $\mathcal{E}_N^{\text{DE}}$ and $\mathcal{E}_N^{\text{MOE}}$ reduce to 0 as P_p increases and the channel estimation becomes error-free. In this case, $\mathcal{E}_N^{\text{DE}}$ is lower than $\mathcal{E}_N^{\text{MOE}}$ and the DE scheme is preferred. Furthermore, the system with more RISs has a lower NMSE-CE than the system with fewer RISs, regardless of the channel estimation scheme. Combining the insights drawn from Fig. 2, we conclude that in the presence of pilot contamination or T-HWIs, the error-free channel estimation cannot be achieved and the MOE scheme outperforms the DE scheme in terms of the NMSE-CE.

B. Performance Enhancement Enabled by RIS

Since the derived SE lower-bounds are the basis and essential tools for acquiring system-design insights, we first evaluate the tightness of the analytical SE lower-bounds for both DE and MOE schemes. Assuming $\kappa_{m,AP}=\kappa_{k,UE}=\kappa,\forall m,\forall k,$

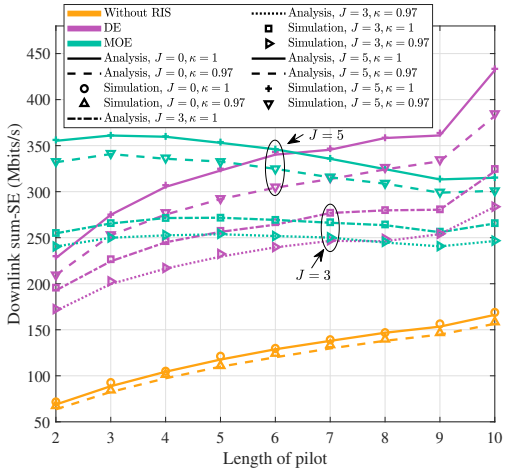

Fig. 4. Downlink sum-SE versus the length of the pilot under different training schemes and degrees of T-HWIs. Here, $M=50$, $K=10$, $N=2$, $L=500$, and $\kappa_{m,AP}=\kappa_{k,UE}=\kappa$.

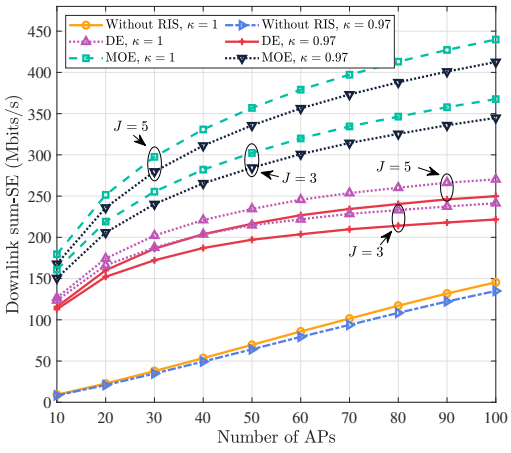

Fig. 5. Downlink sum-SE versus the number of APs under different training schemes and degrees of T-HWIs. Here, $K=10$, $N=2$, $L=500$, $\tau_p=2$, and $\kappa_{m,AP}=\kappa_{k,UE}=\kappa$.

Fig. 4 shows the closed-form sum-SE [i.e., the analytical SE based on Eq. (33)] and the simulated sum-SE [i.e., the ergodic SE according to Eq. (32)] as functions of the length of the pilot τ_p with different degrees of T-HWIs. Note that the simulated sum-SE is generated by averaging over 10^3 independent channel realizations and the sum-SE without RIS (denoted as $\bar{\mathcal{S}}_{sum}$) is obtained by simply letting $J=0$ and $L=0$. The first observation from Fig. 4 is that the analytical SE is in excellent agreement with the simulated SE, which confirms the correctness of the closed-form expressions. In addition, since increasing τ_p reduces the pilot contamination and use of RIS improves the channel propagation, both $\mathcal{S}_{sum}^{\text{DE}}$ and $\bar{\mathcal{S}}_{sum}$ grow as τ_p increases and $\mathcal{S}_{sum}^{\text{DE}}$ is significantly better than $\bar{\mathcal{S}}_{sum}$. Interestingly, $\mathcal{S}_{sum}^{\text{MOE}}$ starts to decrease when τ_p exceeds a threshold. This is because the MOE scheme has a high pilot overhead that grows with τ_p and eventually dominates the SE performance. Despite of having a J-fold increase in pilot overhead compared to the DE scheme, the MOE scheme achieves a remarkable SE gain over the DE scheme in the small-τ_p regime (e.g., $\tau_p \leqslant 6$ for $J=5$ and $\tau_p \leqslant 5$ for $J=3$), as shown in Fig. 4. Moreover, the SE gap widens as τ_p decreases. This result indicates that the proposed MOE scheme is preferred when the pilot resources are scarce. Last but not least, $\mathcal{S}_{sum}^{\text{DE}}$ is more sensitive to T-HWIs than $\mathcal{S}_{sum}^{\text{MOE}}$ and $\bar{\mathcal{S}}_{sum}$. Quantitatively speaking, in the case of $\tau_p=4$, decreasing κ from 1 to 0.97 leads to a 9.86% decrease in $\mathcal{S}_{sum}^{\text{DE}}$, while for $\mathcal{S}_{sum}^{\text{MOE}}$ with $J=5$ and $\bar{\mathcal{S}}_{sum}$, the decreases are only 6.67% and 6.91%, respectively. In what follows, due to the close agreements between the analytical and simulated SEs, we will use the former to conduct the remaining investigation.

Fig. 5 illustrates the impact of increasing the number of APs M on $\mathcal{S}_{sum}^{\text{DE}}$, $\mathcal{S}_{sum}^{\text{MOE}}$, and $\bar{\mathcal{S}}_{sum}$ under different training schemes and degrees of T-HWIs. We observe an apparent gap between $\mathcal{S}_{sum}^{\text{MOE}}$ and $\mathcal{S}_{sum}^{\text{DE}}$, which confirms the advantages of the MOE scheme. Besides, since increasing M provides more multiplexing and array gains, all sum-SEs grow with the increase of M and the largest increase belongs to $\mathcal{S}_{sum}^{\text{MOE}}$. However, using non-ideal hardware leads to the worst SE degradation for $\mathcal{S}_{sum}^{\text{MOE}}$. Even with T-HWIs, $\mathcal{S}_{sum}^{\text{MOE}}$ is still significantly superior to $\mathcal{S}_{sum}^{\text{DE}}$ and $\bar{\mathcal{S}}_{sum}$ with ideal hardware. Interestingly, the RIS-assisted cell-free massive MIMO system with a small number of non-ideal APs outperforms the RIS-free cell-free massive MIMO system with a large number of ideal APs. For instance, in the case of 5 RISs, $\mathcal{S}_{sum}^{\text{MOE}}$ with $M=10$ and $\kappa=0.97$ is 15.37% higher than $\bar{\mathcal{S}}_{sum}$ with $M=100$ and $\kappa=1$, implying that using a few RISs can achieve substantial SE gain and mitigate the impact of T-HWIs.

The behaviors of $\mathcal{S}_{sum}^{\text{DE}}$, $\mathcal{S}_{sum}^{\text{MOE}}$, and $\bar{\mathcal{S}}_{sum}$ varying with different number of elements per RIS L for different degrees of T-HWIs are illustrated in Fig. 6. Once again, $\mathcal{S}_{sum}^{\text{MOE}}$ is much higher than both $\mathcal{S}_{sum}^{\text{DE}}$ and $\bar{\mathcal{S}}_{sum}$. Moreover, given the number of RISs, the SE gain from using more RIS elements (i.e., increasing L) saturates when L reaches a certain threshold, irrespective of the value of κ. This is because in the small L-

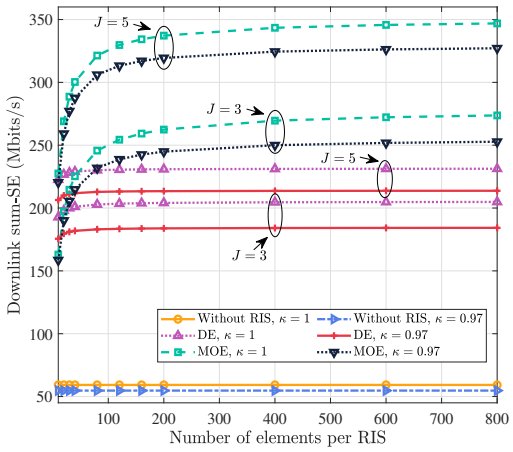

Fig. 6. Downlink sum-SE versus the number of elements per RIS under different training schemes and degrees of T-HWIs. Here, $M=50$, $K=10$, $N=2$, $J=5$, $\tau_p=2$, and $\kappa_{m,AP}=\kappa_{k,UE}=\kappa$.

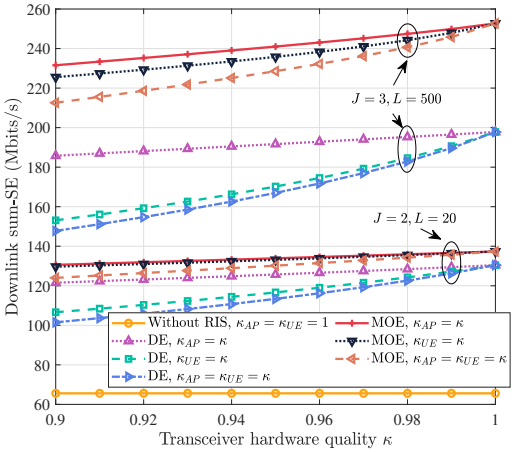

Fig. 7. Downlink sum-SE versus the degree of T-HWIs under different training schemes and numbers of RISs. Here, $M = 50$, $K = 10$, $N = 2$, and $\tau_p = 2$.

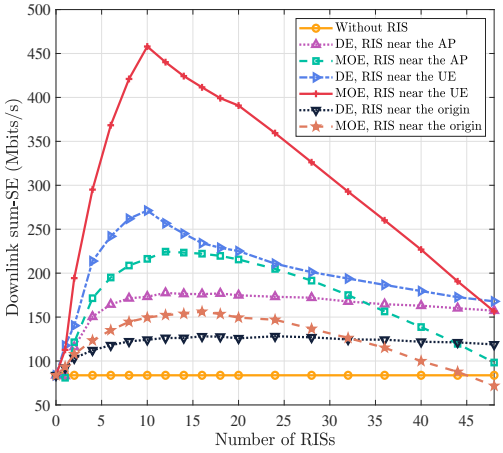

Fig. 8. Downlink sum-SE versus the number of RISs under different training schemes and RIS layouts. Here, $M = 50$, $K = 10$, $N = 2$, $L = 500$, $\tau_p = 2$, $\kappa_{m,AP} = 0.97$, and $\kappa_{k,UE} = 1$.

regime, increasing L provides more RIS paths and naturally enhances the strength of the received signal at the UEs. Nevertheless, since the RIS phase shifts do not affect the SE and the RIS actually acts as a passive relay, using a large number of elements at RIS does not help to refine appropriate beamforming. Therefore, both $\mathcal{S}_{sum}^{\text{DE}}$ and $\mathcal{S}_{sum}^{\text{MOE}}$ converge to specific performance bounds when L is very large. Under such circumstances, the number and the layout of RISs may play important roles in influencing the downlink SE performance.

A common assumption in Figs. 2–6 is $\kappa_{m,AP} = \kappa_{k,UE} = \kappa, \forall m, \forall k$. It is important to investigate whether the non-ideal AP or the non-ideal UE would have a greater impact on the downlink SE performance. To this end, assuming $\kappa_{m,AP} = \kappa_{AP}, \forall m$ and $\kappa_{k,UE} = \kappa_{UE}, \forall k$, Fig. 7 depicts the impact of different κ_{AP} and κ_{UE} on the downlink sum-SE by changing one of the parameters from 0.9 to 1 in steps of 0.01 while keeping the other parameter fixed. Fig. 7 confirms that a higher hardware quality yields a higher sum-SE with and

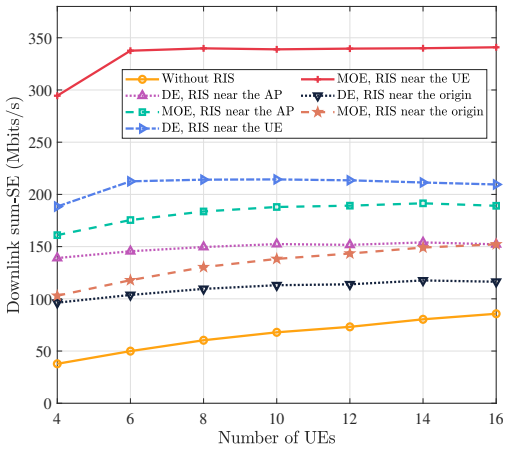

Fig. 9. Downlink sum-SE versus the number of UEs under different training schemes and degrees of T-HWIs. Here, $M = 50$, $N = 2$, $J = 5$, $L = 500$, $\tau_p = 2$, $\kappa_{m,AP} = 0.97$, and $\kappa_{k,UE} = 1$.

without RIS. Besides, for a given product $\kappa_{AP}\kappa_{UE}$, the UE HWIs cause a more severe sum-SE degradation than the AP HWIs regardless of the presence of the RIS, which implies that the downlink SE is mainly limited by κ_{UE}. Therefore, from the perspective of obtaining a better SE, it is preferred to use non-ideal transceivers at the APs rather than at the UEs. Interestingly, we can mitigate the SE degradation by using a few RISs in hardware-impaired cell-free massive MIMO systems. Fig. 7 shows that under scenarios with severe HWIs, using 2 RISs with only 20 elements per RIS is beneficial from the point of view of the SE, making the SE much higher than that of an RIS-free cell-free massive MIMO system with ideal hardware.

We next shed light on the impact of different RIS layouts on the downlink sum-SE under different training schemes and system settings. Figs. 8-10 show the sum-SEs as functions of the number of RISs J, the number of UEs K, and the transmit power of APs P_d, respectively. Note that in addition to the "RIS near the UE" layout used in Figs. 2-7, we also consider two new RIS layouts in Figs. 8-10, i.e., the "RIS near the AP", where the RISs are randomly distributed in the vicinity of the APs with coordinates $\left(x^{\text{AP}} \pm \frac{D}{150}, y^{\text{AP}} \pm \frac{D}{150}\right)$ and the "RIS near the origin" layout, where the RISs are randomly distributed in the vicinity of the origin with coordinates $\left(\pm\frac{D}{150}, \pm\frac{D}{150}\right)$. Simulation results indicate that the "RIS near the UE" layout reaps the best SE performance, followed by the "RIS near the AP" and "RIS near the origin" layouts. Aside from this, there are several interesting findings from Figs. 8-10. Fig. 8 shows that using more RISs help to improve the downlink sum-SE, but the SE gain is of particular significance for MOE-based systems. Besides, $\mathcal{S}_{sum}^{\text{MOE}}$ exhibits a unimodal behavior with respect to J and decreases with increasing J when the pilot overhead is high. Nevertheless, for $J < 46$, $\mathcal{S}_{sum}^{\text{MOE}}$ with the "RIS near the UE" layout surpasses $\mathcal{S}_{sum}^{\text{DE}}$ for all RIS layouts and $\bar{\mathcal{S}}_{sum}$. For $J > 46$, however, the MOE scheme loses its superiority and $\mathcal{S}_{sum}^{\text{MOE}}$ falls below $\mathcal{S}_{sum}^{\text{DE}}$ irrespective of the RIS layout. These results imply that the MOE scheme is

This article has been accepted for publication in IEEE Transactions on Communications. This is the author's version which has not been fully edited and content may change prior to final publication. Citation information: DOI 10.1109/TCOMM.2023.3306890

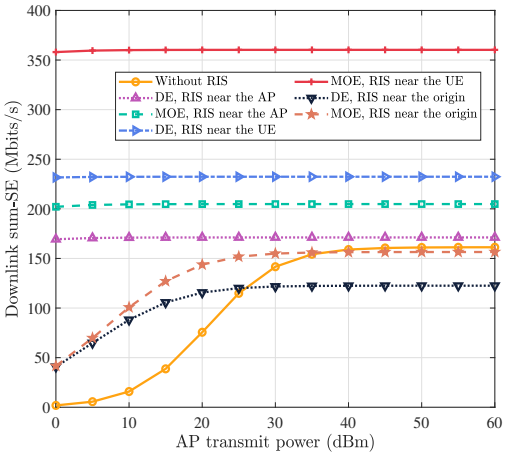

Fig. 10. Downlink sum-SE versus the transmit power of AP under different training schemes and RIS layouts. Here, $M = 50$, $K = 10$, $N = 2$, $J = 5$, $L = 500$, $\tau_p = 2$, $\kappa_{m,AP} = 0.97$, and $\kappa_{k,UE} = 1$.

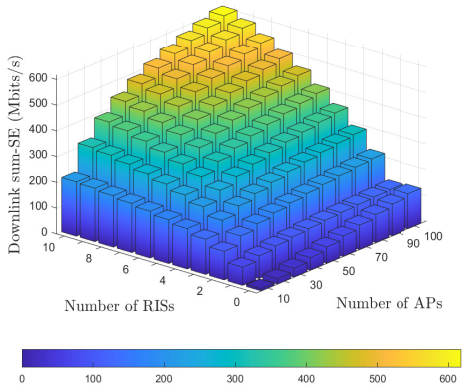

Fig. 11. Downlink sum-SE versus the number of APs and the number of RISs under the MOE scheme. Here, $N = 2$, $L = 500$, $\tau_p = 2$, $\kappa_{m,AP} = 0.97$, and $\kappa_{k,UE} = 1$.

not suitable for systems with a large number of RISs. However, it can achieve a significant SE gain only in cell-free massive MIMO systems with a small number of RISs and limited pilot resources. In addition, Fig. 9 demonstrates that increasing K makes a slight contribution to the sum-SE when $K \geqslant \tau_p$. This is because the increased pilot contamination limits the SE enhancement. However, both $\mathcal{S}_{sum}^{\text{DE}}$ and $\mathcal{S}_{sum}^{\text{MOE}}$ still significantly outperform $\bar{\mathcal{S}}_{sum}$ in the high-K regime. Moreover, Fig. 10 indicates that for scenarios with P_d ranging from 0 to 60 dBm, the sum-SEs with "RIS near the AP" and "RIS near the UE" layouts are barely affected by P_d, which reveals that with proper RIS layouts, we can decrease P_d to the milliwatt level with minimal impact on the sum-SE. Whereas for the RIS-free system and the RIS-assisted system with "RIS near the origin" layout, their sum-SEs grow with the increase of P_d and saturate to fixed capacity bounds when P_d exceeds 40 dBm and 25 dBm, respectively, implying that these systems are interference-limited in the high power regime.

C. Trade-off Analysis Between Using More Hardware-impaired APs and Low-cost RISs

As mentioned earlier, two possible ways to enhance the downlink SE performance of cell-free massive MIMO systems are deploying more hardware-impaired APs or low-cost RISs. Hence, a natural question is which option is more cost-effective. In what follows, we only consider the RIS-assisted cell-free massive MIMO system with the MOE scheme, since it reaps a better SE in most cases. Assuming a small degree of AP HWIs, we depict in Figs. 11 and 12 the three-dimensional surfaces of $\mathcal{S}_{sum}^{\text{MOE}}$ and the total power consumption versus different numbers of APs M and RISs J, respectively. Note that Fig. 12 is obtained by using the aggregated transmit power consumption model $P = M\left(\frac{1}{\alpha}P_d + NP_{tc}\right) + JLP_{RIS}$[4].

[4]This model does not involve the power consumed on the backhaul links and the parameters α, P_{tc}, and P_{RIS} denote the power amplifier efficiency, the internal power required to run the circuit components of each AP, and the power of each RIS element, respectively. Following [42] and [43], we set α=0.4, $P_{tc} = 0.2$ W, and $P_{RIS} = 3.16$ mW with 1-bit RIS phase shifts.

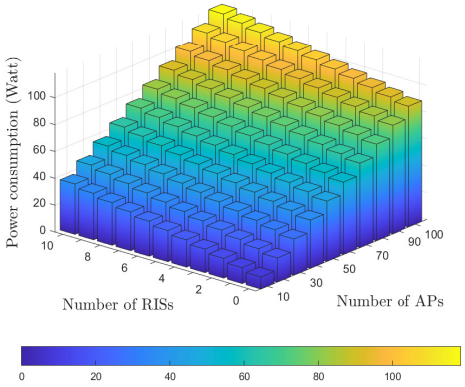

Fig. 12. Power consumption versus the number of APs and the number of RISs under the MOE scheme. Here, $N = 2$, $L = 500$, $\tau_p = 2$, $\kappa_{m,AP} = 0.97$, and $\kappa_{k,UE} = 1$.

Fig. 11 shows that increasing M harvests a more noticeable SE gain than increasing J. Moreover, it is clear that for a given power budget, the RIS-assisted cell-free massive MIMO system with more APs has a lower EE because its SE is much lower than that of the system with more RISs. For instance, the power consumptions of RIS-assisted systems with "$M = 80, J = 1$", "$M = 70, J = 4$", and "$M = 50, J = 10$" are all around 74 Watt, but the sum-SEs of these systems are 132.6, 337.1, and 492.9 Mbits/s, respectively. Undoubtedly, the last system has the best EE. Therefore, it is preferred to deploy more RISs rather than APs to design a cost-effective cell-free massive MIMO system.

VI. Conclusions

We have investigated the downlink SE performance of an RIS-assisted cell-free massive MIMO system with T-HWIs. Based on the LMMSE estimation technique, a novel MOE scheme with moderate pilot overhead is proposed to enhance

the estimation accuracy and SE performance. Taking into account the imperfect CSI and T-HWIs, closed-form expressions of the lower-bound achievable SE with distributed conjugate beamforming are derived. Simulation results demonstrate that the downlink SE of the MOE-based RIS-assisted system significantly surpasses the DE-based RIS-assisted system and the RIS-free system, especially when the RISs are located near the UEs. Moreover, regardless of whether the availability of the RIS, the UE HWIs dominate the downlink SE but their impact can be effectively alleviated by deploying a few RISs. With the help of RIS, the APs can decrease their transmit power to the milliwatt level with negligible SE loss. Furthermore, it is advisable to replace a large number of APs with several RISs to design a more cost-effective cell-free massive MIMO system.

It is worth noting that the channel model considered in this work can be extended to investigate a more practical scenario. For instance, the line-of-sight (LoS) path and RIS spatial correlation may be involved since the RIS is typically mounted on a high building and there is a higher possibility of correlation between its scattering elements. In this case, the RIS phase shifts have an impact on the SE performance and it is worthwhile to design an RIS phase shift optimization scheme. Therefore, future work would incorporate the LoS path, spatial correlation, and phase shift optimization to provide more insights for RIS-assisted cell-free massive MIMO systems.

Appendix A
Proof of Lemma 1

According to [16], the LMMSE channel estimation of $\hat{\boldsymbol{g}}_{mk}$ using the DE scheme is written as

$$\hat{\boldsymbol{g}}_{mk}^{\mathrm{DE}} = \frac{\mathbb{E}\left\{\boldsymbol{g}_{mk}^H \boldsymbol{y}_{mk,p}\right\}}{\mathbb{E}\left\{\left\|\boldsymbol{y}_{mk,p}\right\|^2\right\}} \boldsymbol{y}_{mk,p}. \tag{39}$$

We start with $\mathbb{E}\left\{\left\|\boldsymbol{g}_{mk}\right\|^2\right\}$. Since the direct channels and indirect RIS-assisted channels are uncorrelated with each other, it is easy to find

$$\mathbb{E}\left\{\left\|\boldsymbol{g}_{mk}\right\|^2\right\} = N\left(\beta_{mk}^d + \sum_{j=1}^{J}\sum_{l=1}^{L}\beta_{mj}^d\beta_{kj}^d\right) = N\beta_{mk}. \tag{40}$$

Then, based on Eq. (7) and using the facts that the aggregated channels are uncorrelated with the T-HWIs and CSCG noise and they all have zero mean, we obtain

$$\begin{aligned}\mathbb{E}\left\{\boldsymbol{g}_{mk}^H \boldsymbol{y}_{mk,p}\right\} &= \sqrt{\tau_p\rho_p\kappa_{m,r}}\sum_{k'=1}^{K}\sqrt{\kappa_{k',t}}\boldsymbol{\varphi}_{k'}^H\boldsymbol{\varphi}_k\mathbb{E}\left\{\boldsymbol{g}_{mk}^H\boldsymbol{g}_{mk'}\right\} \\ &\overset{(a)}{=} \sqrt{\tau_p\rho_p\kappa_{m,r}\kappa_{k,t}}\mathbb{E}\left\{\left\|\boldsymbol{g}_{mk}\right\|^2\right\} \\ &= N\sqrt{\tau_p\rho_p\kappa_{m,r}\kappa_{k,t}}\beta_{mk}, \end{aligned} \tag{41}$$

where (a) follows the aggregated channels belonging to different UEs are uncorrelated with each other. Similarly, the denominator of Eq. (39) is calculated as

$$\begin{aligned}\mathbb{E}\left\{\left\|\boldsymbol{y}_{mk,p}\right\|^2\right\} &= \tau_p\rho_p\kappa_{m,r}\sum_{k'=1}^{K}\kappa_{k',t}\left|\boldsymbol{\varphi}_{k'}^H\boldsymbol{\varphi}_k\right|^2\mathbb{E}\left\{\left\|\boldsymbol{g}_{mk'}\right\|^2\right\} \\ &\quad + \kappa_{m,r}\sum_{k'=1}^{K}\kappa_{k',t}\mathbb{E}\left\{\boldsymbol{g}_{mk'}^H\boldsymbol{g}_{mk'}\right\}\mathbb{E}\left\{\boldsymbol{\varphi}_k^H\boldsymbol{\omega}_{k',t}\boldsymbol{\omega}_{k',t}^H\boldsymbol{\varphi}_k\right\} \\ &\quad + \mathbb{E}\left\{\boldsymbol{\varphi}_k^H\boldsymbol{W}_{m,r}^H\boldsymbol{W}_{m,r}\boldsymbol{\varphi}_k\right\} + \mathbb{E}\left\{\boldsymbol{\varphi}_k^H\boldsymbol{N}_{m,p}^H\boldsymbol{N}_{m,p}\boldsymbol{\varphi}_k\right\}. \end{aligned} \tag{42}$$

With the help of Eqs. (4) and (5), we have

$$\mathbb{E}\left\{\boldsymbol{\varphi}_k^H\boldsymbol{\omega}_{k',t}\boldsymbol{\omega}_{k',t}\boldsymbol{\varphi}_k\right\} = \rho_p\left(1-\kappa_{k',t}\right), \tag{43}$$

$$\mathbb{E}\left\{\boldsymbol{\varphi}_k^H\boldsymbol{W}_{m,r}^H\boldsymbol{W}_{m,r}\boldsymbol{\varphi}_k\right\} = N\left(1-\kappa_{m,r}\right)\rho_p\sum_{k'=1}^{K}\beta_{mk'}, \tag{44}$$

$$\mathbb{E}\left\{\boldsymbol{\varphi}_k^H\boldsymbol{N}_{m,p}^H\boldsymbol{N}_{m,p}\boldsymbol{\varphi}_k\right\} = N. \tag{45}$$

Substituting Eqs. (43)–(45) into Eq. (42) and performing some linear operations, $\mathbb{E}\left\{\left\|\boldsymbol{y}_{mk,p}\right\|^2\right\}$ is simplified to

$$\begin{aligned}\mathbb{E}\left\{\left\|\boldsymbol{y}_{mk,p}\right\|^2\right\} &= N\tau_p\rho_p\kappa_{m,r}\sum_{k'\in\mathcal{P}_k}\kappa_{k',t}\beta_{mk'} \\ &\quad + N\rho_p\left(1-\kappa_{m,r}\kappa_{k',t}\right)\beta_{mk'} + N. \end{aligned} \tag{46}$$

Therefore,

$$\begin{aligned}\hat{\boldsymbol{g}}_{mk}^{\mathrm{DE}} &= \frac{\sqrt{\tau_p\rho_p\kappa_{m,r}\kappa_{k,t}}\beta_{mk}}{\tau_p\rho_p\kappa_{m,r}\sum\limits_{k'\in\mathcal{P}_k}\kappa_{k',t}\beta_{mk'} + \rho_p\left(1-\kappa_{m,r}\kappa_{k',t}\right)\beta_{mk'} + 1}\boldsymbol{y}_{mk,p} \\ &= c_{mk}^{\mathrm{DE}}\boldsymbol{y}_{mk,p}. \end{aligned} \tag{47}$$

By virtue of Eqs. (46) and (47), and using the fact that the channel estimation and estimation error are uncorrelated under the LMMSE principle, the norm squares of $\hat{\boldsymbol{g}}_{mk}^{\mathrm{DE}}$ and $\boldsymbol{\varepsilon}_{mk}^{\mathrm{DE}}$ are respectively given as

$$\mathbb{E}\left\{\left\|\hat{\boldsymbol{g}}_{mk}^{\mathrm{DE}}\right\|^2\right\} = N\sqrt{\tau_p\rho_p\kappa_{m,r}\kappa_{k,t}}c_{mk}^{\mathrm{DE}}\beta_{mk} = N\gamma_{mk}^{\mathrm{DE}}, \tag{48}$$

and

$$\mathbb{E}\left\{\left\|\boldsymbol{\varepsilon}_{mk}^{\mathrm{DE}}\right\|^2\right\} = N\left(\beta_{mk}-\gamma_{mk}^{\mathrm{DE}}\right). \tag{49}$$

Thus, the proof for Lemma 1 is finished.

Appendix B
Proof of Theorem 1

Since the derivation of the MOE-based closed-form expression is more complicated than that of the DE-based expression, we only give the derivation steps for $\mathcal{S}_k^{\mathrm{MOE}}$. For notation conciseness, we first rewrite $\hat{\boldsymbol{g}}_{mk}^{\mathrm{MOE}}$ as

$$\begin{aligned}\hat{\boldsymbol{g}}_{mk}^{\mathrm{MOE}} &= \sqrt{\tau_p\rho_p\kappa_{m,r}}\sum_{k'\in\mathcal{P}_k}\bar{\boldsymbol{c}}_{mkk'} + \sqrt{\kappa_{m,r}}\sum_{k'=1}^{K}\bar{\boldsymbol{\omega}}_{mkk'} \\ &\quad + \bar{\boldsymbol{w}}_{mk} + \bar{\boldsymbol{n}}_{mk}, \end{aligned} \tag{50}$$

where

$$\bar{\boldsymbol{c}}_{mkk'} = \sqrt{\kappa_{k',t}}\left(c_{mk}^d\boldsymbol{g}_{mk'}^d + \sum_{j=1}^{J}c_{mkj}^c\bar{\boldsymbol{g}}_{mk'j}^c\right), \tag{51}$$

$$\bar{\boldsymbol{\omega}}_{mkk'} = c_{mk}^d\boldsymbol{g}_{mk'}^d\left(\boldsymbol{\omega}_{k',t}^d\right)^H\boldsymbol{\varphi}_k + \sum_{j=1}^{J}c_{mkj}^c\bar{\boldsymbol{g}}_{mk'j}^c\left(\boldsymbol{\omega}_{k'j,t}^c\right)^H\boldsymbol{\varphi}_k, \tag{52}$$

$$\bar{\boldsymbol{w}}_{mk} = c_{mk}^{d} \boldsymbol{W}_{m,r}^{d} \boldsymbol{\varphi}_k + \sum_{j=1}^{J} c_{mkj}^{c} \boldsymbol{W}_{mj,r}^{c} \boldsymbol{\varphi}_k, \tag{53}$$

and

$$\bar{\boldsymbol{n}}_{mk} = c_{mk}^{d} \boldsymbol{N}_{m,r}^{d} \boldsymbol{\varphi}_k + \sum_{j=1}^{J} c_{mkj}^{c} \boldsymbol{N}_{mj,p}^{c} \boldsymbol{\varphi}_k. \tag{54}$$

Besides, the subscript "MOE" is omitted in the following for ease of exposition. Using the above definitions and by virtue of some linear operations, we can calculate all expectations in Eq. (32) as follows[5].

$$\mathbb{E}\left\{\left|\mathrm{DS}_k\right|^2\right\} = N^2 \rho_d \kappa_{k,r} \left(\sum_{m=1}^{M} \sqrt{\eta_{mk}^{X} \kappa_{m,t}} \gamma_{mk}^{X} \right)^2. \tag{55}$$

$$\begin{aligned}
\mathbb{E}\left\{\left|\mathrm{BU}_k\right|^2\right\} &= N \rho_d \kappa_{k,r} \sum_{m=1}^{M} \kappa_{m,t} \eta_{mk} \left(\beta_{mk} \gamma_{mk} \right. \\
&+ \rho_p \left(1-\kappa_{m,r}\right) \left(\left(\left(c_{mk}^{d} \beta_{mk}^{d}\right)^2 + L^2 \sum_{j=1}^{J} \left(c_{mkj}^{c} \beta_{mkj}^{c}\right)^2 \right) \right. \\
&\quad \left. + L \sum_{j=1}^{J} \left(c_{mkj}^{c}\right)^2 \beta_{mkj}^{c} \sum_{k''=1}^{K} \beta_{mk''j}^{c} \right) \\
&\quad + L \rho_p \left(\tau_p \kappa_{m,r} \kappa_{k,t} + 1 - \kappa_{m,r} \kappa_{k,t}\right) \sum_{j=1}^{J} \left(c_{mkj}^{c} \beta_{mkj}^{c}\right)^2 \Bigg) \\
&\quad + N^2 \rho_d \kappa_{k,r} \sum_{m=1}^{M} \sum_{m'=1}^{M} \sqrt{\kappa_{m,t} \kappa_{m',t} \eta_{mk} \eta_{m'k}} \times \\
&\left(\frac{1-\kappa_{k,t}}{\tau_p \kappa_{k,t}} \left(\gamma_{mk}^{d} \gamma_{m'k}^{d} + \sum_{j=1}^{J} \gamma_{mkj}^{c} \gamma_{m'kj}^{c} \right) + L \rho_p \sqrt{\kappa_{m,r} \kappa_{m',r}} \times \right. \\
&\left. \sum_{k''=1}^{K} \left(\left|\boldsymbol{\varphi}_{k''}^{H} \boldsymbol{\varphi}_{k'}\right|^2 \tau_p \kappa_{k'',t} + 1 - \kappa_{k'',t} \right) \sum_{j=1}^{J} c_{mkj}^{c} c_{m'kj}^{c} \beta_{mkj}^{c} \beta_{m'k''j}^{c} \right).
\end{aligned} \tag{56}$$

$$\begin{aligned}
&\sum_{k' \neq k}^{K} \mathbb{E}\left\{\left|\mathrm{IUI}_{k'k}\right|^2\right\} = N \rho_d \kappa_{k,r} \times \\
&\sum_{k' \neq k}^{K} \left(\sum_{m=1}^{M} \eta_{mk'} \kappa_{m,t} \beta_{mk} \gamma_{mk'} + N \left(\left|\boldsymbol{\varphi}_{k'}^{H} \boldsymbol{\varphi}_{k}\right|^2 + \frac{1-\kappa_{k,t}}{\tau_p \kappa_{k,t}} \right) \times \right. \\
&\left. \left(\sum_{m=1}^{M} \sqrt{\eta_{mk'} \kappa_{m,t}} \left(\gamma_{mk'}^{d} \frac{\beta_{mk}^{d}}{\beta_{mk'}^{d}} + \sum_{j=1}^{J} \gamma_{mjk'}^{c} \frac{\beta_{mkj}^{c}}{\beta_{mk'j}^{c}} \right) \right)^2 \right. \\
&\quad + \rho_p \left(\sum_{m=1}^{M} \eta_{mk'} \kappa_{m,t} \left(1-\kappa_{m,r}\right) \left(\left(c_{mk'}^{d} \beta_{mk}^{d}\right)^2 + L^2 \times \right. \right. \\
&\left. \left. \sum_{j=1}^{J} \left(c_{mk'j}^{c} \beta_{mkj}^{c}\right)^2 \right) + L \sum_{m=1}^{M} \eta_{mk'} \kappa_{m,t} \left(1 - \kappa_{k,t} \kappa_{m,r} \right. \right. \\
&\left. \left. \left. + \tau_p \kappa_{k,t} \kappa_{m,r} \left|\boldsymbol{\varphi}_{k'}^{H} \boldsymbol{\varphi}_{k}\right|^2 \right) \sum_{j=1}^{J} \left(c_{mk'j}^{c} \beta_{mkj}^{c}\right)^2 \right.
\end{aligned}$$

$$\begin{aligned}
&+ L \sum_{m=1}^{M} \eta_{mk'} \kappa_{m,t} \left(1-\kappa_{m,r}\right) \sum_{j=1}^{J} \left(c_{mk'j}^{c}\right)^2 \beta_{mkj}^{c} \sum_{k''=1}^{K} \beta_{mk''j}^{c} \\
&+ NL \sum_{m=1}^{M} \sum_{m'=1}^{M} \sqrt{\kappa_{m,r} \kappa_{m',r} \eta_{mk'} \eta_{m'k'} \kappa_{m,t} \kappa_{m',t}} \sum_{j=1}^{J} c_{mkj}^{c} \times \\
&\left. c_{m'kj}^{c} \beta_{mkj}^{c} \sum_{k''=1}^{K} \beta_{m'k''j}^{c} \left(\left|\boldsymbol{\varphi}_{k''}^{H} \boldsymbol{\varphi}_{k'}\right|^2 \tau_p \kappa_{k'',t} + 1 - \kappa_{k'',t} \right) \right) \Bigg).
\end{aligned} \tag{57}$$

$$\begin{aligned}
\mathbb{E}\left\{\left|\mathrm{THI}_k\right|^2\right\} &= \kappa_{k,r} \mathbb{E}\left\{ \left| \sum_{m=1}^{M} \boldsymbol{g}_{mk}^{T} \boldsymbol{\omega}_{m,t}^{*} \right|^2 \right\} \\
&= N \rho_d \kappa_{k,r} \sum_{m=1}^{M} \left(1-\kappa_{m,t}\right) \sum_{k'=1}^{K} \eta_{mk'} \beta_{mk} \gamma_{mk'}.
\end{aligned} \tag{58}$$

$$\begin{aligned}
&\mathbb{E}\left\{\left|w_{k,r}\right|^2\right\} \\
&= N \rho_d \left(1-\kappa_{k,r}\right) \sum_{k'=1}^{K} \sum_{m=1}^{M} \eta_{mk'} \left(\beta_{mk} \gamma_{mk'} \right. \\
&+ N \left(\left|\boldsymbol{\varphi}_{k'}^{H} \boldsymbol{\varphi}_{k}\right|^2 + \frac{1-\kappa_{k,t}}{\tau_p \kappa_{k,t}} \right) \left(\gamma_{mk'}^{d} \frac{\beta_{mk}^{d}}{\beta_{mk'}^{d}} + \sum_{j=1}^{J} \gamma_{mjk'}^{c} \frac{\beta_{mkj}^{c}}{\beta_{mk'j}^{c}} \right)^2 \\
&+ \rho_p \left(\left(1-\kappa_{m,r}\right) \left(\left(c_{mk'}^{d} \beta_{mk}^{d}\right)^2 + L^2 \sum_{j=1}^{J} \left(c_{mk'j}^{c} \beta_{mkj}^{c}\right)^2 \right) \right. \\
&+ L \left(\tau_p \kappa_{k,t} \kappa_{m,r} \left|\boldsymbol{\varphi}_{k''}^{H} \boldsymbol{\varphi}_{k'}\right|^2 + 1 - \kappa_{k,t} \kappa_{m,r} \right) \sum_{j=1}^{J} \left(c_{mk'j}^{c} \beta_{mkj}^{c}\right)^2 \\
&\quad + L \left(1-\kappa_{m,r}\right) \sum_{j=1}^{J} \left(c_{mk'j}^{c}\right)^2 \beta_{mkj}^{c} \sum_{k''=1}^{K} \beta_{mk''j}^{c} \\
&\quad + NL \kappa_{m,r} \left(\left|\boldsymbol{\varphi}_{k''}^{H} \boldsymbol{\varphi}_{k'}\right|^2 \tau_p \kappa_{k'',t} + 1 - \kappa_{k'',t} \right) \times \\
&\quad \left. \left. \sum_{j=1}^{J} \left(c_{mkj}^{c}\right)^2 \beta_{mkj}^{c} \sum_{k''=1}^{K} \beta_{m'k''j}^{c} \right) \right).
\end{aligned} \tag{59}$$

Plugging Eqs. (55)–(59) into Eq. (32) and performing some algebraic manipulations, Theorem 1 is proved.

[5] Due to page limitation, only the final results are presented.

REFERENCES

[1] H. Q. Ngo, A. Ashikhmin, H. Yang, E. G. Larsson, and T. L. Marzetta, "Cell-free massive MIMO versus small cells," *IEEE Trans. Wireless Commun.*, vol. 16, no. 3, pp. 1834-1850, Mar. 2017.

[2] Y. Zhang, H. Zhao, W. Xia, F. Gao, L. Yang and H. Zhu, "Superimposed pilot transmission in cell-free massive MIMO with non-ideal RF responses," *IEEE Trans. Veh. Technol.*, vol. 71, no. 12, pp. 12856-12868, Dec. 2022.

[3] H. Yang and T. L. Marzetta, "Energy efficiency of massive MIMO: Cell-free vs. cellular," in *Proc. IEEE Veh. Technol. Conf. (VTC)*, Porto, Portugal, 2018, pp. 1-5.

[4] Y. Zhang, W. Xia, G. Zheng, H. Zhao, L. Yang, and H. Zhu, "Secure transmission in cell-free massive MIMO with low-resolution DACs over Rician fading channels," *IEEE Trans. Commun.*, vol. 70, no. 4, pp. 2606-2621, Apr. 2022.

[5] Y. Zhang, W. Xia, H. Zhao, W. Xu, K.-K. Wong, and L. Yang, "Cell-free IoT networks with SWIPT: Performance analysis and power control," *IEEE Internet Things J.*, vol. 9, no. 15, pp. 13780-13793, Aug. 2022.

[6] Q. Wu and R. Zhang, "Intelligent reflecting surface enhanced wireless network via joint active and passive beamforming," *IEEE Trans. Wireless Commun.*, vol. 18, no. 11, pp. 5394-5409, Nov. 2019.

[7] Y. Zhang, H. Zhao, W. Xia, W. Xu, C. Tang, and H. Zhu, "How much does reconfigurable intelligent surface improve cell-free massive mimo uplink with hardware impairments?," *IEEE Trans. Commun.*, pp. 1-17, Aug. 2023, early access, doi: 10.1109/TCOMM.2023.3299970.

[8] C. Huang, A. Zappone, G. C. Alexandropoulos, M. Debbah, and C. Yuen, "Reconfigurable intelligent surfaces for energy efficiency in wireless communication," *IEEE Trans. Wireless Commun.*, vol. 18, no. 8, pp. 4157-4170, Aug. 2019.

[9] L. Wei, C. Huang, G. C. Alexandropoulos, C. Yuen, Z. Zhang, and M. Debbah, "Channel estimation for RIS-empowered multi-user MISO wireless communications," *IEEE Trans. Commun.*, vol. 69, no. 6, pp. 4144-4157, June 2021.

[10] L. Wei, C. Huang, Q. Guo, IEEE, Z. Yang, Z. Zhang, G. C. Alexandropoulos, M. Debbah, and C. Yuen, "Joint Channel estimation and signal recovery for RIS-empowered multiuser communications," *IEEE Trans. Commun.*, vol. 70, no. 7, pp. 4640-4655, July 2022.

[11] L. Wei, C. Huang, G. C. Alexandropoulos, Z. Yang, C. Yuen, and Z. Zhang, "Joint channel estimation and signal recovery in RIS-assisted multi-user MISO Communications," in *Proc. 2021 IEEE Wireless Commun. Netw. Conf. (WCNC)*, 2021, pp. 1-6.

[12] K. Zhi, C. Pan, G. Zhou, H. Ren, M. Elkashlan, and R. Schober, "Is RIS-aided massive MIMO promising with ZF detectors and imperfect CSI?," *IEEE J. Sel. Areas Commun.*, vol. 40, no. 10, pp. 3010-3026, Oct. 2022.

[13] K. Zhi, C. Pan, H. Ren, and K. Wang, "Statistical CSI-based design for reconfigurable intelligent surface-aided massive MIMO systems with direct links," *IEEE Wireless Commun. Lett.*, vol. 10, no. 5, pp. 1128-1132, May 2021.

[14] K. Zhi, C. Pan, H. Ren, and K. Wang, "Ergodic rate analysis of reconfigurable intelligent surface-aided massive MIMO systems with ZF detectors,," *IEEE Commun. Lett.*, vol. 26, no. 2, pp. 264-268, Feb. 2022.

[15] B. Al-Nahhas, M. Obeed, A. Chaaban, and M. J. Hossain, "RIS-aided cell-free massive MIMO: Performance analysis and competitiveness," in *Proc. 2021 IEEE Int. Conf. Commun. Workshops (ICC Workshops)*, 2021, pp. 1-6.

[16] T. Van Chien, H. Q. Ngo, S. Chatzinotas, M. Di Renzo, and B. Ottersten, "Reconfigurable intelligent surface-assisted cell-free massive MIMO systems over spatially-correlated channels," *IEEE Trans. Wireless Commun.*, vol. 21, no. 7, pp. 5106-5128, July 2022.

[17] Q. -U. -A. Nadeem, A. Zappone, and A. Chaaban, "Achievable rate analysis and max-min SINR optimization in intelligent reflecting surface assisted cell-free MIMO uplink," *IEEE Open J. Commun. Soc.*, vol. 3, pp. 1295-1322, 2022.

[18] N. T. Nguyen, V. -D. Nguyen, H. Van Nguyen, H. Q. Ngo, S. Chatzinotas, and M. Juntti, "Spectral efficiency analysis of hybrid relay-reflecting intelligent surface-assisted cell-free massive MIMO systems," *IEEE Trans. Wireless Commun.*, vol. 22, no. 5, pp. 3397-3416, May 2023.

[19] M. Bashar, K. Cumanan, A. G. Burr, P. Xiao, and M. Di Renzo, "On the performance of reconfigurable intelligent surface-aided cell-free massive MIMO uplink," in *Proc. 2020 IEEE Globecom Conf. (GlobeCom2020)*, 2020, pp. 1-6.

[20] Y. Zhang, B. Di, H. Zhang, J. Lin, C. Xu, D. Zhang, Y. Li, and L. Song, "Beyond cell-free MIMO: Energy efficient reconfigurable intelligent surface aided cell-free MIMO communications", *IEEE Trans. Cognitive Commun. Networking*, vol. 7, no. 2, pp. 412-426, June 2021.

[21] Q. N. Le, V. -D. Nguyen, O. A. Dobre, and R. Zhao, "Energy efficiency maximization in RIS-aided cell-free network with limited backhaul," *IEEE Commun. Lett.*, vol. 25, no. 6, pp. 1974-1978, June 2021.

[22] W. Lyu, Y. Xiu, S. Yang, C. Yuen, and Z. Zhang, "Energy-efficient cell-free network assisted by hybrid RISs," *IEEE Wireless Commun. Lett.*, vol. 12, no. 4, pp. 718-722, Apr. 2023.

[23] K. Liu and Z. Zhang, "On the energy-efficiency fairness of reconfigurable intelligent surface-aided cell-free network," in *Proc. 2021 IEEE 93rd Veh. Technol. Conf. (VTC2021-Spring)*, 2021, pp. 1-6.

[24] E. Björnson, J. Hoydis, M. Kountouris, and M. Debbah, "Massive MIMO systems with non-ideal hardware: Energy efficiency, stimation, and capacity limits," *IEEE Trans. Inf. Theor.*, vol. 60, no. 11, pp. 7112-7139, Nov. 2014.

[25] E. Björnson, M. Matthaiou, and M. Debbah, "Massive MIMO with nonideal arbitrary arrays: Hardware scaling laws and circuit-aware design," *IEEE Trans. Commun.*, vol. 14, no. 8, pp. 4353-4368, Aug. 2015.

[26] V. Tentu, E. Sharma, D. N. Amudala, and R. Budhiraja, "UAV-enabled hardware-impaired spatially correlated cell-free massive MIMO systems: Analysis and energy efficiency optimization," *IEEE Trans. Commun.*, vol. 70, no. 4, pp. 2722-2741, Apr. 2022.

[27] Y. Zhang, H. Cao, M. Zhou, L. Li, and L. Yang, "Power optimization in cell-free massive MIMO with non-ideal hardware transceiver," *Chin. J. Electron.*, vol. 29, no. 1, pp. 190-198, Jan. 2020.

[28] X. Zhang, D. Guo, K. An, and B. Zhang, "Secure communications over cell-free massive MIMO networks with hardware impairments," *IEEE Syst. J.*, vol. 14, no. 2, pp. 1909-1920, Jun. 2020.

[29] J. Zheng, J. Zhang, L. Zhang, X. Zhang, and B. Ai, "Efficient receiver design for uplink cell-free massive MIMO with hardware impairments," *IEEE Trans. Veh. Technol.*, vol. 69, no. 4, pp. 4537-4541, Apr. 2020.

[30] A. Papazafeiropoulos, E. Björnson, P. Kourtessis, S. Chatzinotas, and J. M. Senior, "Scalable cell-free massive MIMO systems: Impact of hardware impairments," *IEEE Trans. Veh. Technol.*, vol. 70, no. 10, pp. 9701-9715, Oct. 2021.

[31] H. Masoumi and M. J. Emadi, "Performance analysis of cell-free massive MIMO system with limited fronthaul capacity and hardware impairments," *IEEE Trans Wireless Commun.*, vol. 19, no. 2, pp. 1038-1053, Feb. 2020.

[32] Z. Peng, Z. Chen, C. Pan, G. Zhou, and H. Ren, "Robust transmission design for RIS-aided communications with both transceiver hardware impairments and imperfect CSI," *IEEE Wireless Commun. Lett.*, vol. 11, no. 3, pp. 528-532, Mar. 2022.

[33] Q. Chen, M. Li, X. Yang, R. Alturki, M. D. Alshehri, and F. Khan, "Impact of residual hardware impairment on the IoT secrecy performance of RIS-assisted NOMA networks," *IEEE Access*, vol. 9, pp. 42583-42592, 2021.

[34] Z. Chu, J. Zhong, P. Xiao, D. Mi, W. Hao, R. Tafazolli, and A. P. Feresidis, "RIS assisted wireless powered IoT networks with phase shift error and transceiver hardware impairment," *IEEE Trans. Commun.*, vol. 70, no. 7, pp. 4910-4924, July 2022.

[35] Z. Xing, R. Wang, J. Wu and E. Liu, "Achievable rate analysis and phase shift optimization on intelligent reflecting surface with hardware impairments," in *IEEE Trans. Wireless Commun.*, vol. 20, no. 9, pp. 5514-5530, Sept. 2021.

[36] J. Jose, A. Ashikhmin, T. L. Marzetta, and S. Vishwanath, "Pilot contamination and precoding in multi-cell TDD systems," *IEEE Trans. Wireless Commun.*, vol. 10, no. 8, pp. 2640-2651, Aug. 2011.

[37] D. Mishra and H. Johansson, "Channel estimation and low-complexity beamforming design for passive intelligent surface assisted miso wireless energy transfer," in *Proc. 2019 IEEE Int. Conf. Acoust. Speech Signal Process. (ICASSP)*, 2019, pp. 4659-4663.

[38] D. Mishra and H. Johansson, "Low-complexity beamforming designs and channel estimation for passive-intelligent-surface-assisted MISO energy transfer," *IEEE Internet Things J.*, vol. 10, no. 9, pp. 8286-8304, May 2023.

[39] Y. Zhang, M. Zhou, Y. Cheng, L. Yang, and H. Zhu, "RF impairments and low-resolution ADCs for nonideal uplink cell-free massive MIMO systems," *IEEE Syst. J.*, vol. 15, no. 2, pp. 2519-2530, June 2021.

[40] L. Xu, X. Lu, S. Jin, F. Gao, and Y. Zhu, "On the uplink achievable rate of massive MIMO system with low-resolution ADC and RF impairments," *IEEE Commun. Lett.*, vol. 23, no. 3, pp. 502-505, Mar. 2019.

[41] T. L. Marzetta, E. G. Larsson, H. Yang, and H. Q. Ngo, *Fundamentals of Massive MIMO*. Cambridge, U.K.: Cambridge Univ. Press, 2016.

[42] H. Q. Ngo, L. Tran, T. Q. Duong, M. Matthaiou, and E. G. Larsson, "On the total energy efficiency of cell-free massive MIMO," *IEEE Trans. Green Commun. Netw.*, vol. 2, no. 1, pp. 25-39, Mar. 2018.

[43] C. Huang, G. C. Alexandropoulos, A. Zappone, M. Debbah, and C. Yuen, "Energy efficient multi-user MISO communication using low resolution large intelligent surfaces," in *Proc. 2018 IEEE Globecom Workshops (GC Wkshps)*, 2018, pp. 1-6.

This article has been accepted for publication in IEEE Transactions on Communications. This is the author's version which has not been fully edited and content may change prior to final publication. Citation information: DOI 10.1109/TCOMM.2023.3306890

Yao Zhang (S'17, M'21) received the B.S. degree in network engineering from Qingdao University, China, in 2016, and the Ph.D. degree in communication and information systems from Nanjing University of Posts and Telecommunications, Nanjing, China, in 2021. He is currently with the College of Physics and Electronic Information Engineering, Zhejiang Normal University. His current research interests include massive (large-scale) MIMO systems and performance analysis of fading channels.

Wenchao Xia (S'14, M'19) received his B.S. degree in communication engineering and Ph.D. degree in communication and information systems from Nanjing University of Posts and Telecommunications in 2014 and 2019, respectively. From 2019 to 2020, he was a postdoctoral research fellow at Singapore University of Technology and Design. He is currently with the faculty of the Jiangsu Key Laboratory of Wireless Communications, College of Telecommunications and Information Engineering, Nanjing University of Posts and Telecommunications. His current research interests include edge intelligence, edge computing, cloud radio access networks, and massive MIMO. He was a recipient of the Best Paper Award at IEEE GLOBECOM 2016.

Haitao Zhao (Senior Member, IEEE) received the M.S. degree and the Ph.D. degree (Hons.) in signal and information processing from the Nanjing University of Posts and Telecommunications, Nanjing, China, in 2008 and 2011, respectively. He is currently an Associate Professor with the Nanjing University of Posts and Telecommunications. His current research interests include wireless multimedia modeling, capacity prediction, and wireless network coding.

Gan Zheng (S'05–M'09–SM'12–F'20) received the B.Eng. and M.Eng. degrees in electronic and information engineering from Tianjin University, Tianjin, China, in 2002 and 2004, respectively, and the Ph.D. degree in electrical and electronic engineering from The University of Hong Kong in 2008. He is currently a Reader of signal processing for wireless communications with the Wolfson School of Mechanical, Electrical, and Manufacturing Engineering, Loughborough University, U.K. His research interests include machine learning for communications, UAV communications, mobile edge caching, full-duplex radio, and wireless power transfer. He was a first recipient for the 2013 IEEE Signal Processing Letters Best Paper Award. He received 2015 GLOBECOM Best Paper Award, and 2018 IEEE Technical Committee on Green Communications & Computing Best Paper Award. He currently serves as an Associate Editor for the IEEE COMMUNICATIONS LETTERS. He has been recognized by the Web of Science as a Highly Cited Researcher since 2019. He currently serves as an Associate Editor for IEEE WIRELESS COMMUNICATIONS LETTERS.

Sangarapillai Lambotharan (Senior Member, IEEE) received the Ph.D. degree in signal processing from Imperial College London, U.K., in 1997. Hewas a Visiting Scientist with the Engineering and Theory Centre,Cornell University, USA, in 1996. Until 1999, he was a Postdoctoral Research Associate with Imperial College London. From 1999 to 2002, he was with the Motorola Applied Research Group, U.K., where he investigated various projects, including physical link layer modeling and performance characterization of GPRS, EGPRS, and UTRAN. From 2002 to 2007, he was a Lecturer with King's College London, London, U.K., and a Senior Lecturer with Cardiff University, Cardif, U.K. He is currently a Professor of digital communications and the Head of the Signal Processing and Networks Research Group, Wolfson School of Mechanical, Electrical, and Manufacturing Engineering, Loughborough University, Loughborough, U.K. He has authored 250 journal articles and conference papers in his research areas, which include 5G networks,MIMO, blockchain,machine learning, and network security. He is a Fellow of IET. He is an Associate Editor for IEEE TRANSACTIONS ON SIGNAL PROCESSING and IEEE TRANSACTIONS ON COMMUNICATIONS.

Longxiang Yang received the B.S. degree in electronic engineering from the Xidian University, Xian, China, in 1987, and the Ph.D. degree in precision instrument and mechanics from the Southeast University, Nanjing, China, in 1996. He is currently with the College of Telecommunications and Information Engineering, Nanjing University of Posts and Telecommunications (NJUPT), Nanjing, China. He is a Full Professor and Doctoral Supervisor of NJUPT. He is also the head of College of Telecommunications and Information Engineering, NJUPT. He has fulfilled multiple National Natural Science Foundation projects of China. He has authored and co-authored over 200 technical papers published in various journals and conferences. His research interests include cooperative communication, network coding, wireless communication theory, 5G mobile communication systems, ubiquitous networks and Internet of things.